3
Rocket Propulsion

3.1 Introduction

The types of rocket propulsion and basic parameters used in performance evaluation of rocket propulsion are described in this chapter. First, the concepts of thrust, effective exhaust velocity, and specific impulse are presented for a gaseous continuum leaving a rocket engine. These concepts are covered in more detail than that contained in Chapter 1. To determine the requirements of rocket vehicles, some introductory mechanics of orbital flight are investigated along with rocket mass ratios, rocket acceleration, and multistage rockets. This section on requirements and capabilities is followed by a general discussion of the various sources of rocket propulsion and a summary of their capabilities. Following this general introduction to rocket propulsion and rocket flight is a discussion of rocket nozzle types, a study of the detailed performance parameters for rocket engines expelling a continuum, detailed example problems, and discussion of liquid- and solid-propellant rockets.

3.1.1 Rocket Thrust

The rocket thrust studied here will be applicable to rockets that eject a gaseous continuum material from a nozzle at a constant rate. Chemical and nuclear-H_2 rockets are examples of such rocket propulsion systems. The thrust of an ionic rocket that expels discrete ion particles at high speeds, on the other hand, is not related to properties of a continuum such as pressure and density. The thrust equation to be developed will not apply, therefore, to ionic rockets. The thrust of ion rockets, however, still depends on the same basic principle of operation as chemical or nuclear-H_2 rockets, i.e., the reaction force resulting from imparting momentum to a mass.

3.1.2 Ideal Thrust Equation

The ideal rocket thrust is defined as the force required to hold a rocket at rest as the rocket ejects a propellant rearward under the following assumed conditions:

1) Atmospheric pressure acts everywhere on the rocket's external surface. (There is no interaction between the jet issuing from the rocket nozzle and the air in contact with the external surface of the rocket.)

2) The propellant flows from the rocket at a constant rate in uniform one-dimensional flow at the nozzle exit section.

3) The rate of change of the momentum within the rocket is negligibly small and may be neglected.

The rocket of Fig. 3.1a is held in place by a reaction strut and is ejecting a propellant to the rear under the preceding conditions. The shear force at section B-B of the reaction strut is equal in magnitude to the ideal rocket thrust. As shown by the freebody diagram in Fig. 3.1a, the thrust is produced by the internal force on the rocket shell. In a vacuum, the thrust would be identical with F_{int}, but is less than the internal force in the atmosphere because of the ambient pressure forces acting on the external surface of the rocket. The external force is due to atmospheric pressure forces only and is given by

$$F_{\text{ext}} = P_a A_e$$

If we assume internal isentropic flow, the interior force is due to pressure forces only. It is the sum of all of the pressure forces exerted by the propellant on the interior wall surfaces. The internal force is readily evaluated in terms of propellant flow properties by application of the momentum equation to the control surface indicated in Fig. 3.1b, and by using the fact that the force of the propellant on

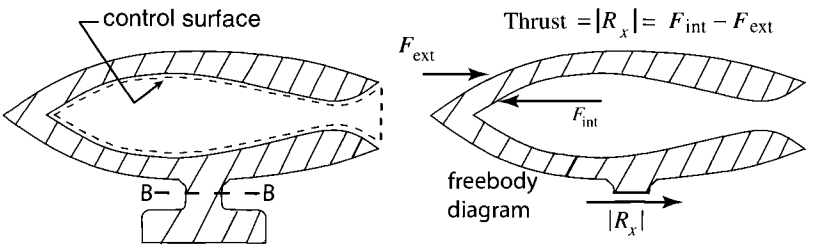

a) Forces on rocket shell

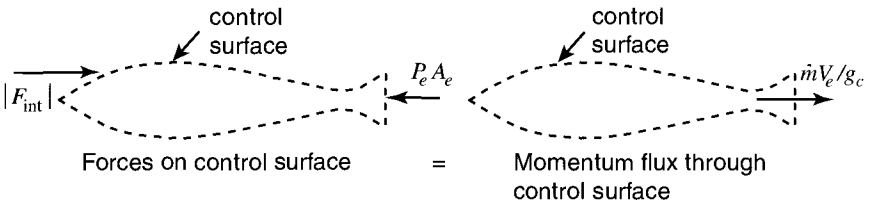

b) Evaluation of $|F_{\text{int}}|$ by momentum equation

Fig. 3.1 Ideal rocket thrust.

the internal walls equals, in magnitude, the force of the walls on the propellant. For the magnitude of the internal force, we obtain

$$|F_{\text{int}}| = P_e A_e + \frac{1}{g_c}\rho_e A_e V_e^2 = P_e A_e + \frac{\dot{m} V_e}{g_c}$$

The difference between F_{int} and F_{ext} is the ideal rocket thrust, F_i,

$$F_i = F_{\text{int}} - F_{\text{ext}}$$

$$F_i = \frac{\dot{m} V_e}{g_c} + (P_e - P_a)A_e \tag{3.1}$$

This equation gives the thrust in terms of the propellant flow properties, the exit area, and the ambient pressure. It is well to remember that only the term $P_a A_e$ on the right side of Eq. (3.1) represents *a real force acting on the rocket shell.*

3.1.3 Optimum Ideal Thrust

Let us consider a rocket ejecting a given propellant supersonically from a combustion chamber at a fixed temperature and pressure. Under these conditions, the mass flow through the rocket nozzle is constant at a value given by

$$\dot{m} = \frac{P_t A}{\sqrt{T_t}} \sqrt{\frac{2 g_c}{R} \frac{\gamma}{\gamma - 1} \left\{ \left(\frac{P}{P_t}\right)^{2/\gamma} - \left(\frac{P}{P_t}\right)^{(\gamma+1)/\gamma} \right\}} \tag{3.2}$$

Let us further assume that the nozzle exit area is adjustable and that the ambient pressure P_a is constant. Now notice that as we vary A_e, the pressure P_e and the velocity V_e will vary, but mass flow rate $\dot{m}$ and P_a will remain constant. The following question arises: For what value of A_e will the corresponding values of V_e and P_e make the thrust of Eq. (3.1) a maximum? The simplest way to demonstrate the optimum thrust condition is to deal with the *real forces* acting on the rocket shell, and to determine directly under what conditions these produce maximum thrust. First, we observe that as A_e is varied by adding a further divergent section on the nozzle exit, any change in thrust comes about by the net force acting on this added section. This follows from the fact that forces acting on the original surfaces of the rocket are not changed by the added section because atmospheric pressure still acts on the original external surfaces, and the original internal pressure distribution remains the same as long as supersonic flow exists at the nozzle exit. Because any thrust change, therefore, comes about by the action of the forces acting on the added surfaces introduced in changing A_e, we need only to examine the forces associated with the added surface to maximize thrust. Figure 3.2 shows an enlarged view of the pressure distribution on the external and internal surfaces near the exit of a rocket nozzle. The external

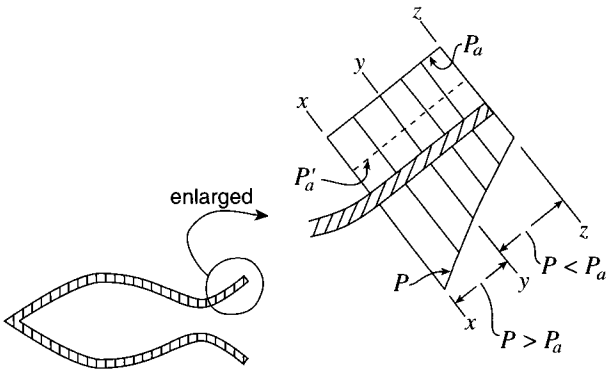

Fig. 3.2 Forces acting on rocket nozzle wall for optimum thrust consideration.

pressure is constant at P_a. The internal pressure decreases from a value greater than P_a at x to P_a at y, and to a value lower than P_a at z, corresponding to an overexpanded nozzle. Now, as A_e is increased by adding surfaces up to station y, we find the thrust is increased because the internal pressure on these added surfaces is greater than P_a. If A_e is increased beyond that value corresponding to y, the thrust is decreased because there is a net drag force acting on the surfaces beyond y because the internal pressure is less than P_a between y and z. To eliminate the wall surface producing a net drag and to not eliminate any wall surface producing a net thrust, the nozzle should be terminated at y where $P_e = P_a$. The exit velocity corresponding to this condition will be denoted $(V_e)_{\text{opt}}$ so that

$$(F_i)_{\text{opt}} = \frac{\dot{m}(V_e)_{\text{opt}}}{g_c} \tag{3.3a}$$

If the nozzle of Fig. 3.2 is at a higher altitude, the ambient pressure is reduced to a value of $P_{a'}$, indicated by the dashed line of Fig. 3.2. The pressure at this higher altitude is such that the internal pressure acting on the nozzle wall from y to z is greater than the new ambient pressure. At this higher altitude, then, the nozzle surface from y to z is a thrust-producing surface and should be retained. This means a higher nozzle area ratio at higher altitudes for optimum thrust.

3.1.4 Vacuum Ideal Thrust

In a vacuum (very high altitudes), $F_{\text{ext}} = 0$. Thus $(F_i)_{\text{vac}} = F_{\text{int}}$, where F_{int} can be evaluated by

$$(F_i)_{\text{vac}} = F_{\text{int}} = \frac{\dot{m}V_e}{g_c} + P_e A_e \tag{3.3b}$$

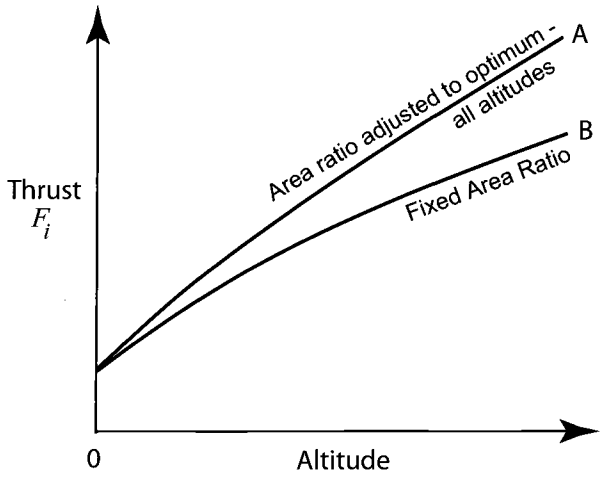

Fig. 3.3 Ideal thrust variation with altitude.

3.1.5 Thrust Variation with Altitude

To understand the variation of thrust with altitude, we consider two rockets, A and B. Rocket A has infinitely adjustable area ratio, whereas rocket B's area ratio is fixed (constant) at a value that gives optimum expansion at sea level.

For each rocket, $F_i = F_{\text{int}} - F_{\text{ext}}$. At higher than sea-level altitudes, rocket A's thrust increases because F_{int} remains the same, and F_{ext} decreases to zero as P_a approaches zero. The thrust of rocket A exceeds that of rocket B at altitudes since F_{ext} decreases the same as for rocket B. In addition, rocket A has thrust-producing surfaces (such as segment x–y of Fig. 3.2) added on to it as it climbs and expands to lower ambient pressures. The variation of thrust for rockets A and B is sketched in Fig. 3.3.

3.1.6 Effective Exhaust Velocity C and Specific Impulse (I_{sp})

The effective exhaust velocity C is defined in Chapter 1 by Eq. (1.53) as

$$C \equiv V_e + \frac{(P_e - P_a)A_e}{\dot{m}/g_c} \tag{3.4}$$

Using this definition of effective exhaust velocity in Eq. (3.1), the ideal thrust is simply

$$F_i = \frac{\dot{m}C}{g_c} \tag{3.5}$$

The values of a rocket's exhaust velocity V_e and exhaust pressure P_e depend on the type of rocket engine and its design and operation. For launch from the

surface of the Earth to Earth orbit, the atmospheric pressure P_a varies from a low of zero (vacuum) to a high of that at sea level. For a rocket engine where the mass flow rate and combustion chamber conditions are constant, the effective exhaust velocity C and ideal thrust F_i will vary from a low value for sea-level operation to a high value at vacuum conditions. Figure 1.42b shows the predicted variation of thrust with altitude for the space shuttle main engine (SSME) under these conditions. The variation of effective exhaust velocity C will be the same as the thrust times a constant. Even though the effective exhaust velocity C can vary, an average value of the effective exhaust velocity may be used for ease of analysis or calculation.

The specific impulse I_{sp} for a rocket is defined as the thrust per unit of propellant weight flow:

$$I_{sp} \equiv \frac{F}{\dot{w}} = \frac{F}{\dot{m}} \frac{g_c}{g_0} \tag{3.6}$$

where g_0 is the acceleration of gravity at sea level. Specific impulse has units of seconds. Using Eq. (3.5), the effective exhaust velocity is directly related to the specific impulse by

$$C = I_{sp} g_0 \tag{3.7}$$

As just discussed, the effective exhaust velocity can vary during operation. From Eq. (3.7), the specific impulse I_{sp} for a rocket engine will vary in direct proportion to its effective exhaust velocity C. For ease of analysis or calculation, an average value of specific impulse may be used.

Example 3.1

Appendix C lists the F-1 engine used on the Saturn V rocket as having a vacuum thrust of 1,726,000 lbf and vacuum I_{sp} of 305 s. Determine the mass flow rate at the vacuum conditions.

Solution: Solving Eq. (3.6) for the mass flow rate, we have

$$\dot{m} = \frac{F}{I_{sp}} \frac{g_c}{g_0} = \frac{1{,}726{,}000}{305} \frac{32.174}{32.174} = 5659 \text{ lbm/s}$$

3.2 Rocket Propulsion Requirements and Capabilities

3.2.1 Requirements

The propulsion requirements for space flight missions are usually expressed in terms of speed increment that the propulsion system must supply to the space vehicle. When the appropriate increment in speed is supplied to a vehicle, the vehicle's guidance system must adjust the direction of the speed to attain the orbit desired. As a simple example, the ideal speed increment to place a

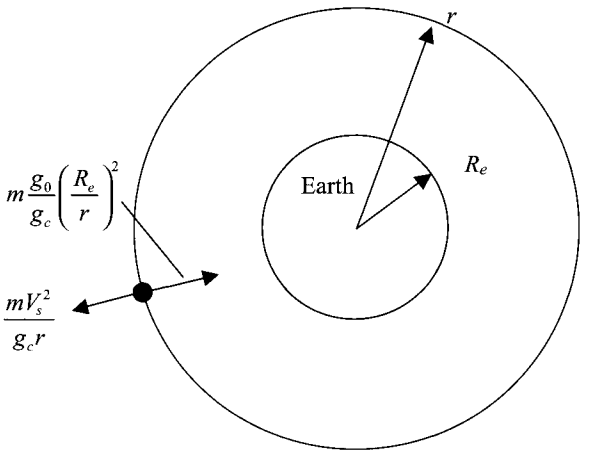

Fig. 3.4 Forces acting on near-Earth-orbiting mass.

vehicle in orbit about the Earth is that speed that will give a balance between the centrifugal and gravitational forces acting on the body in orbit. Considering the balance of these forces, we can determine the needed velocity increment. The force of gravity acting on a mass m at a distance r from the Earth's center is $m\frac{g_0}{g_c}\left(\frac{R_e}{r}\right)^2$, where R_e is the Earth's radius (3959 miles, 6370 km), and g_0 is the acceleration of gravity on the surface of the Earth (32.174 ft/s^2, 9.807 m/s^2). Referring to the force diagram of Fig. 3.4, we have

$$\frac{mV_s^2}{g_c r} = m\frac{g_0}{g_c}\left(\frac{R_e}{r}\right)^2$$

Solving for the satellite velocity V_s at a height h above the surface of the Earth ($r = R_e + h$) gives

$$V_s = \sqrt{g_0 \frac{R_e^2}{R_e + h}} \tag{3.8}$$

For a circular Earth orbit at 160 km (100 miles), Eq. (3.8) gives a satellite velocity of 7800 m/s (25,600 ft/s). Thus a rocket must increase the velocity from zero at launch to 7800 m/s at 160 km. The propulsion system's fuel is the original source of the kinetic energy and the higher potential energy possessed by the orbital mass of Fig. 3.4. The kinetic energy (KE) of the orbital mass is simply given by $\{mV_s^2/(2g_c)\}$, and the change in potential energy (ΔPE) is given by

$$\Delta\text{PE} = \int_{R_e}^{R_e+h} m\frac{g}{g_c}\,\mathrm{d}r = mR_e^2\frac{g_0}{g_c}\int_{R_e}^{R_e+h}\frac{\mathrm{d}r}{r^2} = m\frac{g_0}{g_c}\left(\frac{R_e}{R_e+h}\right) \tag{3.9}$$

The sum of the changes in potential and kinetic energies per unit mass $\{\Delta(\text{pe} + \text{ke})\}$ of the orbiting mass relative to sea-level launch is given by

$$\Delta(\text{pe} + \text{ke}) = \frac{\Delta(\text{PE} + \text{KE})}{m} = \frac{g_0}{g_c}\left(\frac{R_e}{R_e + h}\right) + \frac{V_s^2}{2\,g_c} \tag{3.10}$$

To place a mass in circular Earth orbit at 100 miles requires that the sum of the potential and kinetic energies be increased by 13,760 Btu/lbm (32 MJ/kg). This energy change is equal to the kinetic energy of a mass at a velocity of 26,250 ft/s (8000 m/s). In addition to this energy, the propulsion system must supply the energy that is delivered to the viscous atmosphere by the ascending vehicle due to aerodynamic drag forces. Thus the equivalent velocity increment requirement of a propulsion system to attain a near Earth orbit is greater than 26,250 ft/s (8000 m/s) due to aerodynamic drag. Taking these items into account gives an equivalent velocity increment requirement of approximately 30,000 ft/s (9140 m/s) for a near Earth orbit. Table 3.1 gives this velocity increment and those required for certain other space missions.

To escape the Earth's gravitational field ($h \to \infty$), solution of Eq. (3.9) gives the change in potential energy as Earth escape:

$$\Delta\text{pe} = \frac{g_0}{g_c} R_e \tag{3.11}$$

This potential energy change is equal to the kinetic energy corresponding to the escape velocity V_{escape} given by

$$V_{\text{escape}} = \sqrt{2\,g_0 R_e} \tag{3.12}$$

Comparison of Eq. (3.12) for the escape velocity to Eq. (3.8) for the satellite velocity evaluated for low Earth orbit gives

$$V_{\text{escape}} = \sqrt{2} V_s \tag{3.13}$$

This equation explains why the velocity increment of 42,000 ft/s (12,800 m/s) required for Earth escape (see Table 3.1) is 12,000 ft/s (3660 m/s) higher than that required for low Earth orbit.

Table 3.1 Mission equivalent velocity increment requirements

Mission	ΔV_{equiv} (m/s)	ΔV_{equiv} (ft/s)
Low Earth orbit	9,140	30,000
Earth escape-lunar hit	12,800	42,000
High Earth orbit	13,720	45,000
Lunar orbit		
Mars, Venus Probe		
Lunar soft landing	15,240	50,000
Lunar round trip	18,280	60,000
Escape from solar system		

The total mass of a rocket vehicle is the sum of its parts. For convenience, the vehicle mass is considered to be divided into three different masses: the payload mass m_{pl}, the propellant mass m_p, and the remaining mass, which will be called the dead weight mass m_{dw}. The mass of the structure includes the rocket engines, guidance and control system, tankage, rocket structure, etc. The initial mass of a rocket vehicle, m_o, can be expressed as

$$m_o = m_{\text{pl}} + m_p + m_{\text{dw}} \tag{3.14}$$

For convenience, we define the payload mass ratio λ and dead weight mass ratio δ as

$$\lambda \equiv \frac{m_{\text{pl}}}{m_o} \quad \text{and} \quad \delta \equiv \frac{m_{\text{dw}}}{m_o} \tag{3.15}$$

If all of the propellant is consumed during firing, the resulting vehicle mass is defined as the burnout mass m_{bo}, or

$$m_{\text{bo}} = m_o - m_p = m_{\text{pl}} + m_{\text{dw}} \tag{3.16}$$

In addition to the mass ratios of Eq. (3.15), the vehicle mass ratio (MR) is defined as the initial mass m_o divided by the burnout mass m_{bo}, or

$$\text{MR} \equiv \frac{m_o}{m_{\text{bo}}} \tag{3.17}$$

Using Eq. (3.16) and the mass ratio defined in Eq. (3.15), the MR can be written as

$$\text{MR} = \frac{1}{\lambda + \delta} \tag{3.18}$$

3.2.2 Equation of Motion for an Accelerating Rocket

In this section, the velocity increment ΔV of a rocket is related to the propulsion system's burning time t_b, the ejected mass velocity V_e, and the space vehicle's MR. The equation of motion for an accelerating rocket (see Fig. 3.5) rising from the Earth under the influence of gravity and drag as it expels matter was developed in Chapter 1. The analysis resulted in the general expression for the differential velocity change given by Eq. (1.58), or

$$\mathrm{d}V = -C\frac{\mathrm{d}m}{m} - \left(\frac{D}{m/g_c} + g\cos\theta\right)\mathrm{d}t \tag{3.19}$$

where C is the effective exhaust velocity. For launch from the surface of the Earth, the acceleration of gravity g can be written in terms of the radius from the center of the Earth, r, the acceleration of gravity at sea level, g_0, and the

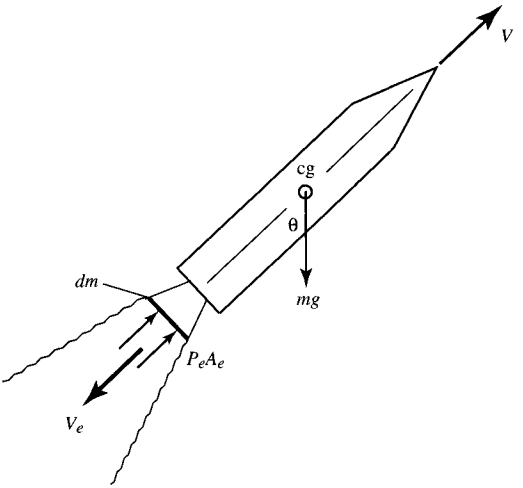

Fig. 3.5 Accelerating rocket.

radius of the Earth, R_e, as follows:

$$g = g_0\left(\frac{R_e}{r}\right)^2$$

Substitution of this expression into Eq. (3.19) yields

$$dV = -C\frac{dm}{m} - \left\{\frac{D}{m/g_c} + g_0\left(\frac{R_e}{r}\right)^2 \cos\theta\right\}dt \tag{3.20}$$

In this equation, dV is the velocity increment supplied to the vehicle of mass m in time dt as mass dm is expelled rearward at effective velocity C relative to the vehicle. Notice that dm is a negative quantity for leaving mass and hence $-C(dm/m)$ becomes a positive number exceeding the

$$\left\{\frac{D}{m/g_c} + g_0\left(\frac{R_e}{r}\right)^2 \cos\theta\right\}dt$$

when values of C are sufficiently high to produce a positive increment in V. When dm is zero (no burning), dV becomes a negative until the kinetic energy possessed by the vehicle at burnout is all converted into potential energy of the vehicle at zero velocity and maximum height. After this condition is reached, the vehicle begins to descend, and its potential energy is converted back into kinetic energy that, in turn, is dissipated into the atmosphere during reentry. To avoid this simple yo-yo motion, we assume that a guidance system has the rocket follow a specified trajectory. The trajectory is such that the vehicle's velocity vector is perpendicular to the radius r at the instant of burnout, and a near Earth orbit is established corresponding to the velocity of 26,000 ft/s.

Integration of Eq. (3.20) from liftoff to burnout gives us the desired relation between the vehicle's velocity increment ΔV and the propulsion system's burning time t_b, the effective exhaust velocity C, the drag D, the trajectory, and the vehicle's MR. Thus

$$\Delta V = \int_0^{V_\infty} \mathrm{d}V = -\int_{m_o}^{m_{\mathrm{bo}}} C\frac{\mathrm{d}m}{m} - g_o \int_{t=0}^{t_{\mathrm{bo}}} \left\{ \frac{D/m}{g_0/g_c} + \left(\frac{R_e}{r}\right)^2 \cos\theta \right\} \mathrm{d}t \tag{3.21}$$

where subscript bo denotes burnout conditions. Evaluation of this equation requires detailed knowledge of the trajectory and vehicle drag.

Using Eq. (3.21), the effective velocity increment $\Delta V_{\mathrm{effective}}$, the drag velocity increment ΔV_{drag}, and gravity velocity increment $\Delta V_{\mathrm{gravity}}$ are defined by

$$\begin{aligned} \Delta V_{\mathrm{effective}} &\equiv -\int_{m_o}^{m_{\mathrm{bo}}} C\frac{\mathrm{d}m}{m} \\ \Delta V_{\mathrm{drag}} &\equiv g_c \int_{t=0}^{t_{\mathrm{bo}}} \left\{\frac{D}{m}\right\} \mathrm{d}t \\ \Delta V_{\mathrm{gravity}} &\equiv g_o \int_{t=0}^{t_{\mathrm{bo}}} \left\{ \left(\frac{R_e}{r}\right)^2 \cos\theta \right\} \mathrm{d}t \end{aligned} \tag{3.22}$$

Note that the effective velocity increment $\Delta V_{\mathrm{effective}}$ is the specific vehicle impulse (engine thrust per unit mass of the vehicle integrated over time), or

$$\Delta V_{\mathrm{effective}} \equiv -\int_{m_o}^{m_{\mathrm{bo}}} C\frac{\mathrm{d}m}{m} \equiv \int_{t=0}^{t_{\mathrm{bo}}} \frac{\dot{m}C}{m}\,\mathrm{d}t \equiv g_c \int_{t=0}^{t_{\mathrm{bo}}} \frac{F}{m}\,\mathrm{d}t \tag{3.23}$$

Equation (3.21) for the vehicle's velocity increment can be rewritten as

$$\Delta V = \Delta V_{\mathrm{effective}} - \Delta V_{\mathrm{drag}} - \Delta V_{\mathrm{gravity}} \tag{3.24}$$

This equation shows the effect of drag and gravity on effective velocity increment that was discussed earlier in this section, namely, that the effective velocity increment $\Delta V_{\mathrm{effective}}$ is greater that the vehicle's velocity increment ΔV due to vehicle drag losses and gravity.

Assuming constant effective exhaust velocity C, Eq. (3.22) gives the following expression for effective velocity increment:

$$\Delta V_{\mathrm{effective}} = C\ell n\left(\frac{m_o}{m_{\mathrm{bo}}}\right) = C\ell n(\mathrm{MR}) = C\ell n\left(\frac{1}{\lambda+\delta}\right) \tag{3.25}$$

Equation (3.25) is plotted in Fig. 3.6, which shows the exponential relationship between the mass ratio and the effective velocity ratio ($\Delta V_{\mathrm{effective}}/C$). Both Fig. 3.6 and Eq. (3.25) show the extreme sensitivity of the mass ratio to the effective exhaust velocity for a given high energy mission (large $\Delta V_{\mathrm{effective}}$).

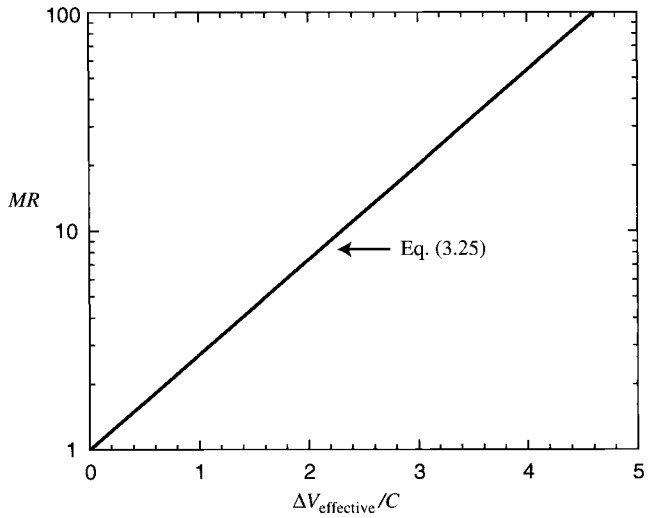

Fig. 3.6 Ideal rocket vehicle mass ratio.

Many space missions require multiple $\Delta V_{\text{effective}}$. Consider a mission from Earth orbit to the surface of the moon and return. This mission will require at least six ΔV: one to exit Earth orbit and reach transit speed; a second to enter lunar orbit; a third to land on the moon; a fourth to reach lunar orbit again; a fifth to exit lunar orbit and reach transit speed; and a sixth to enter Earth orbit. Additional ΔV will be required for trajectory corrections, vehicle orientation, etc. Each ΔV expends vehicle mass, and the mass ratio (m_o/m_{bo}) for the total mission of a single-stage vehicle can be obtained using Eq. (3.25) where $\Delta V_{\text{effective}}$ is the sum of all of the effective velocity changes $(\Delta V_{\text{effective}})$ in the mission.

For a near Earth orbit, R_e/r is close to unity ($R_e = 3959$ miles, $r = 3959 + 100 = 4059$ miles, and $R_e/r = 0.975$), and $\Delta V_{\text{gravity}}$ can be approximated as $\Delta V_{\text{gravity}} \approx g_0 t_{\text{bo}}$. Assuming constant effective exhaust velocity C and negligible drag ($\Delta V_{\text{drag}} = 0$), Eqs. (3.24) and (3.25) give

$$\Delta V = V_{\text{bo}} = C\ell n\left(\frac{m_o}{m_{\text{bo}}}\right) - g_0 t_{\text{bo}} \tag{3.26}$$

This simple equation provides a means of comparing the performance of different propulsion systems in terms of vehicle gross mass m_o required to put a given mass m_{bo} into a low Earth orbit requiring a vehicle velocity increment of V_{bo}.

Example 3.2

To demonstrate the importance of a high propellant exhaust velocity V_e, let us determine the orbital payload capabilities of various propulsion systems for a fixed initial vehicle gross weight. Table 3.2 gives approximate representative values of effective exhaust velocity C for four propulsion systems. The dead

Table 3.2 Performance of high-thrust rocket propulsion systems

Propulsion system fuel and propellant	Effective exhaust velocity, C		Assumed dead weight ratio (δ)
	m/s	ft/s	
Solid	2440	8000	0.03
Liquid O_2-kerosene (RP)	3050	10,000	0.03
Liquid O_2 and H_2	4110	13,500	0.06
Nuclear fuel using H_2 propellant	8230	27,000	0.10

weight ratio δ listed consists of tankage, pumps, and structural members excluding the payload.

As a reference point, we determine first the gross weight at liftoff for a 2000-lbm payload placed in a near Earth orbit by a liquid O_2-kerosene propulsion system. At burnout, the payload, m_{pl}, and the rocket dead weight, m_{dw}, have attained the velocity V_{bo} and both will orbit. Therefore,

$$m_{bo} = m_{pl} + m_{dw} = m_{pl} + \delta m_o = m_{pl} + 0.03\, m_o$$

We will assume for each propulsion system that the burning time is 100 s. We have, from Eq. (3.26),

$$\text{MR} = \frac{m_o}{m_{bo}} = \frac{m_o}{m_{pl} + 0.03\, m_o} = \exp\left\{\frac{V_{bo} + g_o t_{bo}}{C}\right\}$$

$$\text{MR} = \frac{m_o}{m_{bo}} = \frac{m_o}{2000 + 0.03\, m_o} = \exp\left\{\frac{30{,}000 + 3217}{10{,}000}\right\} = \exp\{3.32\} \approx 28$$

Thus

$$m_o = 28\{2000 + 0.03\, m_o\} = 56{,}000 + 0.84\, m_o$$

$$m_o = 56{,}000/0.16 = 350{,}000 \text{ lbm}$$

Thus to place a 2000-lbm payload in a near Earth orbit requires a sea-level liftoff gross weight of 350,000 lbf. With this gross weight as a reference point, let us evaluate the orbiting payload capabilities of the other propulsion systems of Table 3.2.

For the propulsion system using liquid O_2 and H_2, we find a pad weight of 350,000 lbf is capable of placing 8890 lbm into a near Earth orbit. The computation follows:

$$m_{pl} = m_{bo} - m_{dw} = m_o\left\{\exp\left(-\frac{V_{bo} + g_o t_{bo}}{C}\right) - 0.06\right\}$$

$$m_{pl} = 350{,}000\left\{\exp\left(-\frac{33{,}217}{13{,}500}\right) - 0.06\right\} = 350{,}000(0.0854 - 0.06)$$

$$m_o = 8890 \text{ lbm}$$

Table 3.3 Near-Earth orbital payload for 350,000 lbm (158,760 kg) launch mass

	Solid propellant	Liquid O_2-RP	Liquid H_2-O_2	Nuclear-H_2
C (ft/s)|(m/s)	8000|2440	10,000|3050	13,500|4115	27,000|8230
δ (dead weight ratio)	0.03	0.03	0.06	0.10
Payload (lbm)|(kg)	Nothing	2000|907	8890|4040	67,000|30,390
λ (payload ratio)	−0.0142	0.0057	0.0250	0.1914

Similar calculations give the results shown in Table 3.3. The solid-propellant propulsion system's performance is not sufficient to place any mass in orbit under the assumed conditions. The results in Table 3.3 indicate that a high value of effective exhaust velocity is extremely beneficial, if not mandatory. An increase in C by a factor of 2.7, in going from LOX-RP to nuclear-H_2, permits a 33-fold increase in the payload even though the dead weight of the nuclear-H_2 system is three times that of the LOX-RP propulsion unit. Obviously, it is advantageous to have a high exhaust velocity.

3.2.3 Rocket Vehicles in Free Space

When rockets are fired in "free space," there are no drag or gravitational penalties. Integration of Eq. (3.21) under these conditions and assuming constant effective exhaust velocity C yields

$$\Delta V/C = \ell n(\mathrm{MR}) = \ell n\left(\frac{1}{\lambda + \delta}\right) \tag{3.27a}$$

or

$$\mathrm{MR} = \frac{1}{\lambda + \delta} = \exp(\Delta V/C) \tag{3.27b}$$

For rocket vehicles in free space, the effective velocity increment $\Delta V_{\text{effective}}$ equals the vehicle's velocity increment ΔV, and thus Fig. 3.6 is also a plot of Eq. (3.27b).

3.2.4 Multiple-Stage Rocket Vehicles

The launch of a payload using single-stage rocket vehicles was investigated in the previous section. When large energy changes are required (large ΔV) for a given payload, the initial vehicle mass of a single-stage vehicle and its associated cost become very enormous. We consider a liquid H_2-O_2 chemical rocket ($C = 4115$ m/s, 13,500 ft/s) launching a 900-kg (2000-lbm) payload on a mission requiring a ΔV of 14,300 m/s (46,900 ft/s). From Fig. 3.6 or Eq. (3.27b), the required vehicle MR is 32.30. This high mass ratio for a payload of 900 kg and 3% dead weight results in an initial vehicle mass of 938,000 kg mass and

a vehicle dead weight mass of about 29,070 kg. This large initial vehicle mass can be dramatically reduced by using a multistage vehicle.

For a multistage vehicle with N stages, the payload of a lower stage, $[m_{pl}]_i$, is the mass of all higher stages, $[m_o]_{i+1}$, or

$$[m_{pl}]_i = [m_o]_{i+1} \qquad \text{for } i < N \tag{3.28}$$

From Eq. (3.27b), the initial mass of stage i and above (denoted by $[m_o]_i$) is given by

$$[m_o]_i = \frac{1}{\exp\{-(\Delta V/C)_i\} - \delta_i}[m_{pl}]_i \tag{3.29a}$$

and the payload ratio of stage i (denoted by λ_i) is given by

$$\lambda_i = \exp\{-(\Delta V/C)_i\} - \delta_i \tag{3.29b}$$

Using Eq. (3.27a), the total velocity change, ΔV_{total}, for an N-stage rocket can be written as

$$\Delta V_{\text{total}} = \sum_{i=1}^{N} C_i \ell n\left(\frac{1}{\lambda_i + \delta_i}\right) \tag{3.30}$$

The overall payload ratio λ_o for a multistage rocket is the product of all the λ_i and can be expressed as

$$\lambda_o = \prod_{i=1}^{N} \lambda_i \tag{3.31}$$

Equations (3.28) and (3.29) can be used to obtain the mass ratio required for each stage i of a multistage rocket.

Example 3.3

Consider both a two-stage vehicle and a three-stage vehicle for the launch of the 900-kg (2000-lbm) payload. Each stage uses a liquid H_2-O_2 chemical rocket ($C = 4115$ m/s, 13,500 ft/s), and the ΔV_{total} of 14,300 m/s (46,900 ft/s) is split evenly between the stages. Because each stage has the same ΔV and effective exhaust velocity C, the payload ratio λ_i of the stages of a multistage vehicle are the same. The payload ratio for a stage λ_i is 0.1460 for a two-stage vehicle and 0.2840 for a three-stage vehicle. Table 3.4 summarizes the results for one-, two-, and three-stage vehicles. Note that a very large reduction in initial vehicle mass is obtained when going from a single-stage vehicle to a two-stage vehicle (a two-stage vehicle is 4.5% of the mass of the single-stage vehicle), and only a slight reduction in mass is obtained going from a two-stage vehicle to a three-stage vehicle (a three-stage vehicle is 93% of the mass of the two-stage vehicle).

Table 3.4 Multistage vehicle sizes for a 900-kg payload at a ΔV of 14,300 m/s with liquid H_2-O_2

	Single-stage vehicle	Two-stage vehicle	Three-stage vehicle
Stage ΔV	14,300 m/s	7150 m/s	4,767 m/s
Stage δ_i	0.03	0.03	0.03
Stage λ_o	0.0009590	0.02130	0.02290
Vehicle m_o	938,480 kg	42,250 kg	39,300 kg
1st Stage m_{dw}	28,170 kg	1,270 kg	1,180 kg
1st Stage m_{pl}	900 kg	6,170 kg	11,200 kg
2nd Stage m_o		6,170 kg	11,200 kg
2nd Stage m_{dw}		185 kg	336 kg
2nd Stage m_{pl}		900 kg	3,180 kg
3rd Stage m_o			3,180 kg
3rd Stage m_{dw}			95 kg
3rd Stage m_{pl}			900 kg

3.3 Rocket Propulsion Engines

Figure 3.7 shows the basic features of any propulsion system. The function of the propulsion system is to combine energy with matter to produce a directed stream of high-speed particles. That portion of the propulsion system that performs this function may be called the accelerator. In most systems, it is necessary to transport the propellant to the accelerator, and this implies pumps and a certain amount of plumbing. In some systems, it is necessary to supply the propellant in a special form. For example, the ion accelerator requires the propellant in the form of an ionized gas. We lump all of these functions under the heading Propellant Feed System in Fig. 3.7. In all propulsion systems, it is necessary to convert the energy stored onboard the vehicle into a form that is compatible with the particular mechanisms used to accelerate the exhaust particles. Thus there must be an energy conversion system as shown in Fig. 3.7. The energy conversion system may range from a single combustion chamber, wherein the energy of chemical bonds is released, to a nuclear-electric power plant. For the purposes of further discussion, we divide propulsion systems into two broad categories: 1) thermal systems and 2) electric systems.

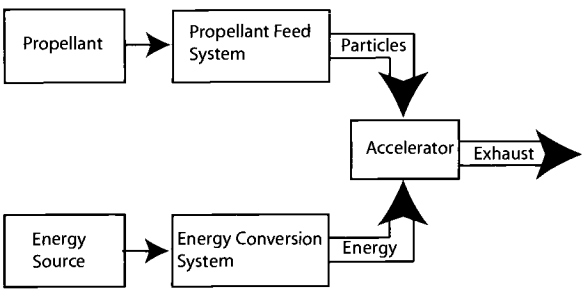

Fig. 3.7 Basic features of a rocket propulsion system.

3.3.1 Thermal Propulsion Systems

The basic principle of a thermal propulsion system is the paragon of simplicity. Energy from a chemical reaction, or from a nuclear reactor, or even from an electric arc discharge, is used to elevate the temperature of the propellant. The individual particles of the propellant thereby obtain considerable kinetic energy in the form of random thermal motion. The propellant is then expanded through a convergent-divergent nozzle whose purpose is to convert the random thermal energy of the propellant into a more or less unidirectional stream of high-speed particles. In this context, a thermal system is a hot gas generator with a nozzle for an accelerator. The nozzle-accelerator simply tries to make an ordered state of affairs out of the chaos of random thermal motion.

A key parameter in the analysis of propulsion systems in general is specific impulse I_{sp}. Thermodynamic analysis indicates, under some ideal assumptions, that the specific impulse of a thermal system is proportional to the quantity $T_c/\mathcal{M}$, where T_c is the propellant combustion chamber temperature and $\mathcal{M}$ is its molecular weight. To produce a high specific impulse in a thermal system, it is then desirable to have a high operating temperature in connection with a low molecular weight of exhaust products. The extent to which these two desirable objectives can be achieved is a rough basis for comparing thermal propulsion systems.

3.3.1.1 Chemical propulsion systems. Chemical propulsion systems are a subclass of thermal systems that use the energy released by exothermic chemical reaction in a combustion chamber. Chemical systems may be further divided into liquid-bipropellant engines, solid-propellant engines, and hybrid engines.

Figure 3.8a shows the essential features of a liquid rocket system. Two propellants (an oxidizer and a fuel) are pumped into the combustion chamber. The hybrid engine is shown in Fig. 3.8b, and the propellant is a solid fuel around the combustion chamber. We may summarize this system as follows:

1) Energy conversion system—combustion chamber,
2) Propellant feed system—fuel pump, oxidizer pump, and gas turbine (not required in hybrid system),
3) Accelerator—nozzle.

Figure 3.9 shows the essential features of a solid-propellant propulsion system. In this case, the fuel and oxidizer are mixed together and cast into a

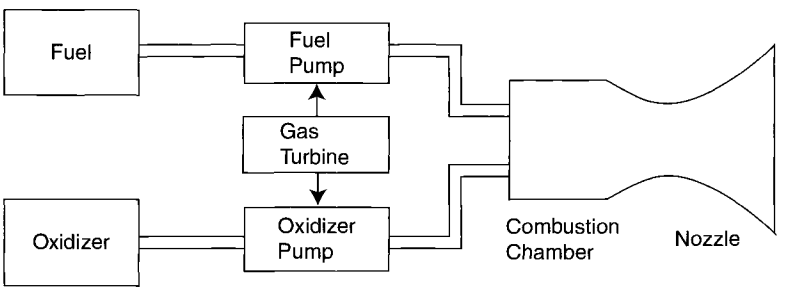

Fig. 3.8a Liquid-bipropellant rocket engine.

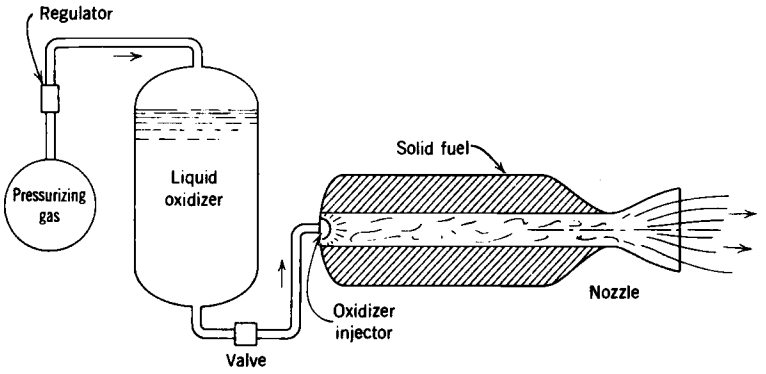

Fig. 3.8b Hybrid propulsion rocket engine.

solid mass called the grain. The grain is usually formed with a hole down the middle called the perforation and is firmly cemented to the inside of the combustion chamber. After ignition, the grain burns radially outward, and the hot combustion gases pass down the perforation and are exhausted through the nozzle.

We may summarize a solid-propellant system as follows:

1) Energy conversion system—combustion chamber
2) Propellant feed system—none
3) Accelerator—nozzle

The absence of a propellant feed system in the solid-propellant chemical rocket is one of its outstanding advantages.

Table 3.5 gives the pertinent characteristics of several different chemical propellants. It is important to note that the combustion temperature T_c and the molecular weight of exhaust products, $\mathcal{M}$, are largely determined by the specific chemical reaction taking place in the combustion chamber. It is possible to select different combinations and thereby achieve an increase in specific impulse, but there are limitations because the products of chemical combustion inherently tend to have relatively high molecular weights.

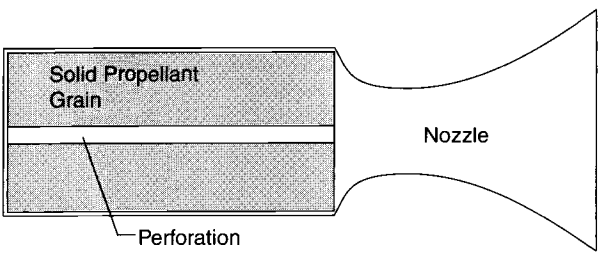

Fig. 3.9 Solid-propellant rocket engine.

Table 3.5 Characteristics of chemical propellants

Oxidizer and fuel	T_c, K	$\mathscr{M}$	I_{sp}, s
O_2-kerosene	3400	22	260
O_2-H_2	2800	9	360
F_2-H_2	3100	7.33	400
Nitrocellulose	2300–3100	22–28	200–230

This discussion serves to point out an important characteristic of chemical propulsion systems, namely, the oxidizer and fuel serve as both the source of energy and the source of particles for the propulsion system. Thus the process of supplying energy to the accelerator and the process of supplying particles to the accelerator are closely related. These fundamental facts place an upper bound of about 400 s on the specific impulse I_{sp} obtainable by chemical means.

3.3.1.2 Nuclear heat transfer propulsion systems. Figure 3.10 shows the essential features of the nuclear heat transfer propulsion system. As the name suggests, this system contains a nuclear reactor that serves two important purposes: 1) it produces the energy necessary to heat the propellant gas to a high temperature; 2) it transfers this energy to the propellant gas. Thus the reactor serves both as an energy source and a heat exchanger. Once heated in the reactor, the hot propellant gas is expanded through a nozzle in the manner characteristic of all thermal systems. The major components of this system are:

1) Energy conversion system—solid core nuclear reactor
2) Propellant feed system—pump and turbine
3) Accelerator—nozzle

An important feature of the nuclear heat transfer system is that the source of exhaust particles and the source of energy are independent. The propellant supplies the particles and the reactor supplies the energy. Thus the propellant need not be selected on the basis of its energy content, but can be selected on the basis of its suitability as exhaust material for a thermal propulsion system. In other words, the primary consideration in the selection of a propellant is low molecular weight.

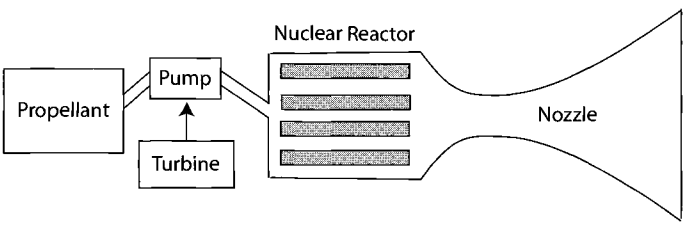

Fig. 3.10 Nuclear heat transfer propulsion system.

Table 3.6 Characteristics of propellants for nuclear propulsion

Propellant	T_c, K	$\mathcal{M}$	Max I_{sp}, s
H_2	2800	2	1000
C_3H_8 (propane)	2800	5.8	530
NH_3 (ammonia)	2800	8.5	460

Table 3.6 lists some important characteristics of different propellants for nuclear propulsion. Note that hydrogen produces the highest specific impulse because it has the lowest molecular weight. This fact is the primary reason that hydrogen is most often mentioned as the propellant for nuclear systems. Note also that the temperature T_c is the same for all three propellants listed in the table. The temperature T_c is determined primarily by the structural limitations of the reactor-heat exchanger and not by the nature of the propellant.

3.3.1.3 Electrothermal propulsion systems. Electrothermal propulsion systems use electric power to heat a propellant gas. One method of doing this is to pass the propellant around an electric arc as suggested by Fig. 3.11. The resulting propulsion system is sometimes called a thermal arcjet. A second possibility is to use tungsten heater elements (temperature increased by electrical energy) as a mechanism for imparting thermal energy to the propellant. In either case, the propellant can be heated to a rather high temperature, perhaps as high as 10,000 K. The temperature could be made higher, but beyond about 10,000 K, a significant portion of the input energy is used up in ionization and disassociation of the atoms of the propellant. This energy (called 'frozen flow' losses) is, therefore, not available for the basic purpose of the device, which is to impart kinetic energy to a directed stream of particles. We should also add that at very high temperatures, the exhaust stream would contain significant pieces of the electrodes and nozzle. These two effects alone tend to place an upper bound on the temperature to which the propellant may be heated, and hence there is an upper bound (~2500 s) on the specific impulse of the electrothermal devices. The major components of the system are:

1) Energy conversion system—electric plant and arc chamber
2) Propellant feed system—propellant pump
3) Accelerator—nozzle

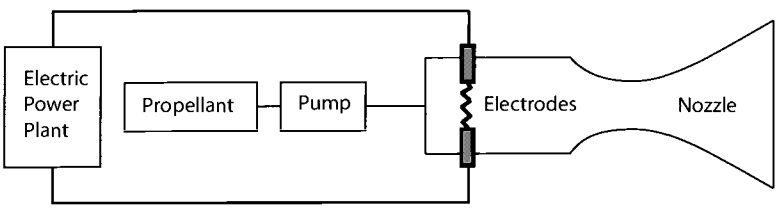

Fig. 3.11 Thermal arcjet propulsion system.

The electrothermal system is also characterized by the fact that the propellant plays no part in the process of supplying energy to the accelerator. The system also requires an electric power plant in the energy conversion system, and this feature is an important consideration in the design of vehicles propelled by electrothermal means. Because of the electric power plant, this system is often classified as an electric propulsion system. We have called it a thermal system because of the characteristic pattern of a high temperature gas plus expansion through a nozzle.

3.3.2 Electric Propulsion Systems

Electric propulsion systems are characterized by an accelerator that makes use of the interaction of electromagnetic fields and charged particles. In a rather crude sense, the electric charge on a particle provides a way for an electromagnetic field to regulate and direct the motion of the particle. In particular, it is possible to accelerate the particle to a high speed and eject it from a rocket vehicle. As should be clear by now, the ejection of high-speed particles is the very essence of rocket propulsion.

This simple picture of an electric propulsion system conceals some rather basic subtleties. First, the propellant feed system for such a system must do more than merely transport the propellant to the accelerator. It must also operate on the propellant to produce significant amounts of ionized particles at the entrance to the accelerator. Second, we note that electromagnetic fields are capable of accelerating charged particles to a very high specific impulse. However, it is necessary to supply the energy to the accelerator in electric form, and hence it is necessary to carry an electric power plant along on the mission. The electric power plant is the key to the problem because estimates of the power level for propulsion run into the megawatt range. In other words, the energy conversion system for an electric propulsion system is quite likely to be a very large and massive device. We will have more to say about this shortly.

3.3.2.1 Electromagnetic propulsion systems. Electromagnetic systems use a magnetic field to accelerate a collection of gas, called a plasma, to a speed on the order of 50,000 m/s (150,000 ft/s). A plasma is a fully or partially ionized gas containing essentially equal numbers of electrons and ions. Because the plasma is a rather good conductor of electricity, it will interact with electromagnetic fields. Because the plasma is also a gas, it displays the properties of a continuum or fluid. As a result, the basic description of the interaction of a magnetic field and a plasma combines all of the pleasantries of electromagnetic field theory and fluid mechanics into a whole new field of study called magnetohydrodynamics (MHD), or sometimes, magnetofluidmechanics.

In this new field, it is quite possible to write down the governing equations, but it is quite another matter to solve them. The factors involved in the study of MHD include the electrical and fluid properties of the plasma, the time history of the magnetic field (e.g., pulsed or continuous), and the geometry of the accelerator. The upshot of all of this is that there are MHD forces acting on the plasma. These

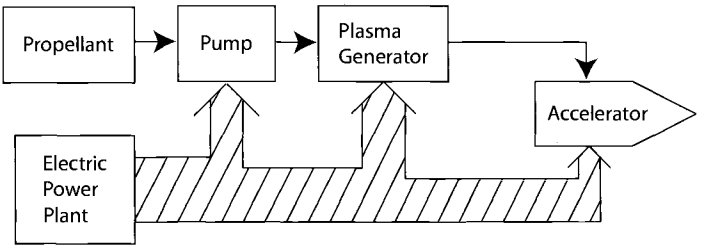

Fig. 3.12 Plasma propulsion system.

forces may act on the boundary of the plasma or may be distributed throughout the volume. In any case, the basic problem is to use these forces to drive the plasma out of the vehicle and thereby produce useful propulsive thrust.

Because of the variety of ways in which MHD forces can be made to act on a plasma, there is a bewildering array of plasma accelerators. The list of devices is constantly growing, and it is quite hopeless to try to classify them in any simple way that would do justice to the subject. In this case, we must be content with the schematic picture of the electromagnetic system shown in Fig. 3.12. We should recognize that the plasma generator and plasma accelerator shown in the figure represent a variety of possible devices. However, they are all united by the joint feature of using the action of a magnetic field on a macroscopically neutral plasma. The major components of the system are:

1) Energy conversion system—electric power plant
2) Propellant feed system—pump and plasma generator
3) Accelerator—plasma accelerator

The names MHD propulsion and plasma propulsion are often associated with this system. Although the specific impulse range for this system is not definitely established, the range 2,000–10,000 s is a reasonable consensus of the values given in open literature. Hydrogen, helium, and lithium are mentioned as propellants.

There is an important feature of the plasma system that is well worth mentioning at this point. The exhaust stream of this system is electrically neutral, and hence the neutralization problems of the ion engine, which we discuss next, are avoided in this case.

3.3.2.2 Electrostatic propulsion systems. The operating principle of this system is based on the static electric fields to accelerate and eject electrically charged particles. Figure 3.13 shows the main features of an ion engine. The propellant introduced into the engine is electrically neutral because charged particles cannot be stored in appreciable amounts. The ions are produced immediately before they are exposed to the accelerating field. This is accomplished by stripping off one or more electrons from the neutral propellant molecule, which is then a single- or multiple-charged positive ion. The positive ion is then accelerated by the electric field and ejected from the engine at a high speed. During this process of acceleration, it is necessary to focus and shape the ion beam to minimize the number of collisions between the ions and the structural members of the engine. Finally, both ions and electrons must be ejected from the engine to keep it

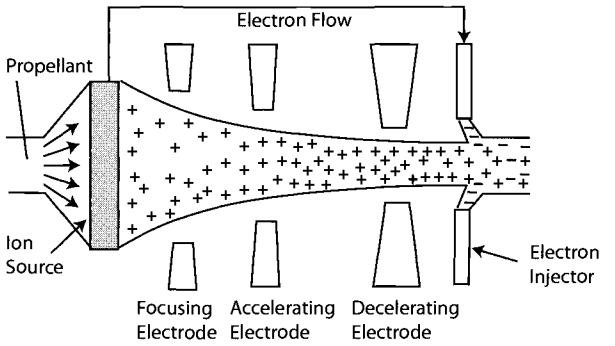

Fig. 3.13 Sketch of ion engine (electrostatic accelerator).

electrically neutral. This is accomplished by gathering up the electrons available at the ion source and transporting them to the engine exit where they are injected into the ion stream, thus hopefully producing an electrically neutral propulsive beam. The three major parts of an ion engine are the ion source, accelerator section, and beam neutralizer (electron injector).

In the simplest terms, a charged particle acquires a kinetic energy equal to its loss of electric potential energy when it "falls" through a difference in electric potential. This basic idea leads to the following expression for the exhaust speed on an ion engine:

$$\frac{1}{2}m_i V_e^2 = q\Delta v \tag{3.32}$$

where

Δv = net accelerating voltage, V
q = electric charge on the ion, C
m_i = mass of the ion, kg
V_e = exhaust speed, m/s

The factors affecting the exhaust speed are the net accelerating voltage Δv and the charge to mass ratio q/m_i of the exhausted particles.

To have a compact, efficient engine, it is desirable to have a rather high accelerating voltage, something on the order of several tens of thousands of volts. With this constraint in mind, we can investigate the influence of charge-to-mass ratio on the selection of the propellant.

Example 3.4

If we assume 1) that the ions are protons (disassociated and ionized hydrogen, $q/m_i = 0.91 \times 10^8$ C/kg) and 2) a reasonable accelerating voltage of 10,000 V, we obtain an exhaust speed of 1.34×10^6 m/s. This corresponds to a specific impulse of 134,000 s.

This value of specific impulse is several orders of magnitude higher than that obtainable from thermal systems. Thus it appears that the ion engine can produce incredibly high specific impulses.

However, several other considerations enter the picture to modify this apparently rosy situation. Performance analysis indicates there is an upper bound on the specific impulse so that the system has the capability of accomplishing useful missions. The reasons for this upper bound and the various factors involved will not emerge until one takes up the discussion of rocket performance. It suffices to say, at this point, that the ion engine is capable of producing specific impulses that are too high to be useful, and that a reasonable upper bound on specific impulse is something on the order of 100,000 s.

This situation points out one of the very profound differences between ion propulsion and thermal propulsion. In the latter, the propellant is often selected to make the specific impulse as high as possible. With ion propulsion, the problem is to select a propellant that will hold the specific impulse (at reasonable accelerator voltages) down to a useful value. For this reason, our interest centers on the heavier elements in the periodic table.

An additional consideration is the fact that the propellant must be supplied to the accelerator in ionized form, and this involves the expenditure of a certain amount of energy that is, therefore, not available for the purpose of propulsion. The amount of energy required for this purpose is measured by the ionization potential of an atom. Table 3.7 gives some important properties of the alkali metals. The alkali metals are the most promising propellants, because they combine the desirable features of low ionization potential together with reasonable accelerating voltages at useful specific impulses.

Figure 3.14 shows a schematic diagram of an electrostatic propulsion system. The major components may be identified as:

1) Energy conversion system—electric power plant
2) Propellant feed system—pump and ion source
3) Accelerator—ion engine

For obvious reasons, this system is also called an ion propulsion system. The preceding discussion points out there is an upper limit on the specific impulse for an ion system. It will also be difficult to obtain efficient operation at lower specific impulses as well. This lower limit arises due to a number of practical considerations such as electrode erosion at low accelerator voltages and

Table 3.7 Characteristics of propellants for electrostatic propulsion

Propellant	First ionization potential, ev	Atomic weight	Accelerating voltage at $I_{sp} = 10^5$ s
Sodium	5.14	23	12,000 V
Rubidium	4.18	85.4	45,000 V
Cesium	4.89	133.0	69,000 V

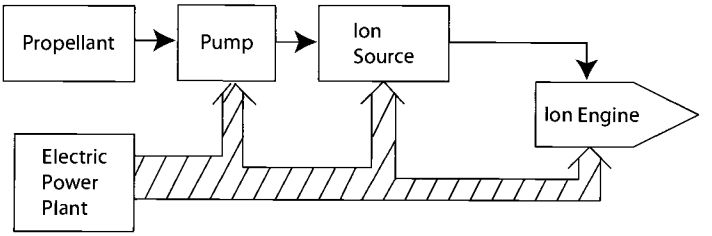

Fig. 3.14 Major features of an electrostatic (ion) propulsion system.

radiation from the hot surfaces of the ion source. The lower limit appears to be about 7500 s.

3.3.2.3 Electric power plants for space propulsion. A major component in any electric propulsion system is the electric power plant, and so we examine the situation regarding the generation of power in space. Electrical power will be required for a variety of reasons, including communication, control, life support, and propulsion. There are a great many methods of power generation that could satisfy some of these needs. Our interest is the generation of electric power for the purposes of propulsion. The very stringent requirements of electric propulsion narrow the field of interest.

One important factor is the power levels of interest in electric propulsion. For Earth satellite missions, such as altitude control, the power levels are on the order of 50–100 kW. More ambitious missions, such as lunar flight, require 1–3 MW. Manned interplanetary flight will require 20–100 MW of electric power. As a matter of perspective, we note that the installed capacity of Hoover Dam is 1200 MW. In other words, we are talking about electric power plants that are comparable to Earth-bound station applications that must operate for long periods of time in the rather unfriendly environs of space.

Our discussion will center on two parameters of space power plants: efficiency and specific mass α_c. Specific mass is defined as the mass of the power plant per unit output (electrical) power, or

$$\alpha_c = \frac{m_c}{P_c} \tag{3.33}$$

where

α_c = the specific mass, kg/W
P_c = the electrical output power, W
m_c = the total mass of the power plant, kg

All space power plants consist of at least three basic elements: an energy source, a conversion device, and a waste heat radiator. The only two energy sources that seem to offer much hope of producing the power levels of interest are the sun and the nuclear fission reactor. Solar collectors for the megawatt range become extremely large and must be constructed in a very sophisticated (i.e., flimsy) manner. Such

devices could stand only very small accelerations, and meteorite erosion of polished surfaces would be a problem. Nuclear power reactors are very powerful sources of energy. They have the important advantage that the power output is limited primarily by the capability of the reactor coolant to remove heat. They have a low specific mass and long life at high power levels. On the other hand, the reactor produces a radiation hazard for the crew and payload.

Both the solar collector and the nuclear reactor produce thermal energy. Among the possible methods of converting thermal energy into electrical energy are the following: thermionic, thermoelectric, and turboelectric. These three methods of conversion use vastly different mechanisms, but all three have one common feature—very low efficiency.

The inefficiency of power conversion schemes results in an increase in the specific mass of the power plant for two important reasons. First, the overall size and mass of the energy source must be increased to "supply" the losses. Second, the losses must somehow be dumped overboard by a waste heat rejection system. For the times of operation and power levels of interest in space propulsion, the only mechanism available for the rejection of heat waste is radiation into space. Because of the inherent low efficiency of the system, the waste heat radiator will be a very large and massive device. It will be susceptible to meteorite puncture and the attendant loss of working fluid from the system. For many designs, it appears that the waste heat radiator will be the dominant mass in the power plant for outputs exceeding a few hundred kilowatts.

Table 3.8 gives some projected characteristics of space power plants. As we have noted, all of the systems have low efficiency. The values of specific mass given in the table should be taken as tentative, particularly in the 1–10 MW range, because systems of this power level have not been built. Authorities differ widely in their estimate of the situation, and there is considerable uncertainty in the figures.

In all of this, we should not lose sight of the fact that the purpose of the propulsion system is to impart kinetic energy to a directed stream of particles. In electric propulsion, this energy first appears as thermal energy and then must be converted into electrical energy before it is in a form suitable for the basic task at hand. As we have suggested, the process of converting thermal energy into electricity in space is not noted for its efficiency. For the foreseeable future, it appears that electric propulsion will continue to pay a severe penalty for the several conversion processes involved in the generation of electric power. It is no exaggeration to state that the use of electric propulsion will be paced by the development of lightweight, efficient power conversion systems.

Table 3.8 Characteristics of space power systems

		Specific mass – α_c (kgm/W)	
System	Efficiency	10–100 kW	1–10 MW
Turboelectric	10–20%	0.02–0.04	0.003–0.004
Thermionic	5–10%	0.5–1.0	0.003–0.004
Thermoelectric	5–10%	0.5–1.0	—

3.3.3 Summary of Propulsion Systems

There are a number of ways in which propulsion systems can be classified to indicate certain fundamental features. In our discussion, we have used the classifications of *thermal* and *electric*. This classification is based on the mechanism used by the accelerator to impart kinetic energy to the exhaust stream. Thus propulsion systems may be summarized as follows.

Thermal:
1) Chemical
2) Nuclear heat transfer
3) Electrothermal (thermal arc jet)

Electric:
1) Electrostatic (ion)
2) Electromagnetic (plasma)

There are other fundamental features of propulsion systems of no less importance, and consideration of these leads to other possible classifications. For example, in our discussion, we noted that in certain systems, the propellant does not supply energy to the accelerator. That is, the source of energy and the source of particles are separate. Such propulsion systems are called separately powered. On the basis of this feature, we have the following classification.

Separately powered:
1) Nuclear heat transfer
2) Electrothermal (thermal arc jet)
3) Electromagnetic (plasma)
4) Electrostatic (ion)

Non-separately powered:
1) Chemical

Note that the chemical propulsion system is termed non-separately powered because the propellant supplies both energy and particles to the accelerator.

Propulsion systems can also be classified according to their performance capabilities as measured by the two key parameters, I_{sp} and thrust-to-weight (sea-level-weight) ratio. Table 3.9 presents typical values of these quantities for various propulsion systems.

The data in Table 3.9 offer several new ways to classify propulsion systems. For example, specific impulse values range over a fairly continuous spectrum from 200 (the lower end of the chemical range) up to 100,000 (the upper end

Table 3.9 Rocket performance summary

Propulsion system	I_{sp}, s	Thrust-to-weight ratio
Chemical	300–400	up to 10^2
Nuclear heat transfer	400–1000	up to 30
Electrothermal	400–2500	up to 10^{-2}
Electromagnetic	2000–10^4	up to 10^{-3}
Electrostatic	7500–10^5	up to 10^{-4}

of the ion range). Thus the order in which the systems are listed in Table 3.9 is a classification based on magnitude of specific impulse. There is, of course, some overlap, but in large measure, each of the systems fills a gap in the specific impulse spectrum.

A very important distinction between propulsion systems is found in Table 3.9. Note that there are several orders of magnitude difference between the thrust-to-weight ratio of electric propulsion systems and the chemical or nuclear propulsion systems. This leads to a classification of systems as either high thrust or low thrust.

High-thrust systems:
1) Chemical
2) Nuclear heat transfer

Low-thrust systems:
1) Electrothermal
2) Electromagnetic
3) Electrostatic

Note that all of the low-thrust systems require an electric power plant as the energy conversion system. This fact accounts for the low values of thrust-to-weight ratios for these systems. Significant increases in the thrust-to-weight capabilities of these systems can be achieved only by reducing the weight-per-unit power of space power plants.

Figure 3.15 is a summary of propulsion systems obtained by plotting the data in Table 3.9. Notice the very clear distinction between the high-thrust and low-thrust systems. Notice also that there is a fairly continuous range of specific impulse capability from 200 to 100,000 s with some significant overlapping among the electric propulsion systems.

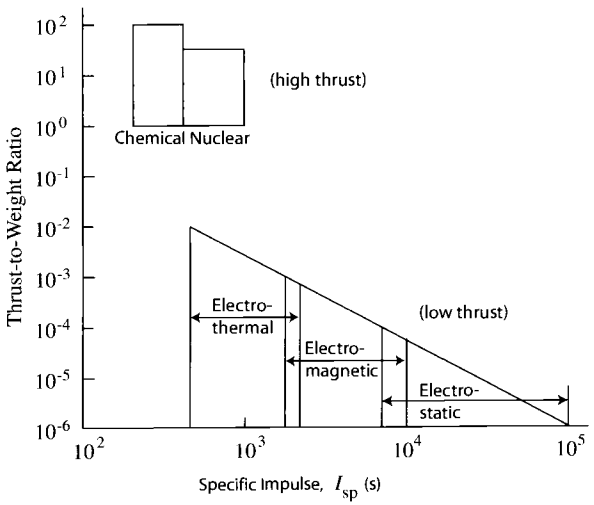

Fig. 3.15 Thrust-to-weight ratio vs specific impulse.

3.4 Types of Rocket Nozzles

The initial geometry of a circular-section rocket nozzle is fixed by the nozzle inlet, throat, and exit areas. The inlet area A_c is established by combustion chamber design considerations. The throat and exit areas are determined from a knowledge of the combustion chamber temperature and pressure, acceptable mean values of γ and R, the propellant mass flow rate, and the designed nozzle-pressure ratio $P_c/P_a = P_c/P_e$. With these data, the nozzle throat and exit areas can be obtained by application of the mass flow parameter (MFP). Having established A_c, A_t, and A_e (or the radii R_c, R_t, R_e), the problem of the nozzle contour design remains. Because of weight and space limitations, determination of the nozzle shape reduces to the problem of choosing a contour providing minimum length (a measure of volume and weight) and yielding maximum thrust. In addition, the selected contour must be sufficiently simple to manufacture.

3.4.1 Conical Nozzle

The conical nozzle represents a compromise of the length, thrust, and ease of manufacturing design criteria weighted somewhat in favor of the last factor. A conical nozzle consists of two truncated cones (Fig. 3.16), joined top to top along their axis by a suitable radius to form the nozzle throat. The combustion chamber is similarly faired into the convergent nozzle section. The converging contour of the nozzle is not critical as regards the flow, and a rather rapid change in cross section is permissible here with a conical apex half-angle on the order of 400 commonly used. The divergence angle of the supersonic portion of the nozzle, however, is limited by flow separation considerations and must not exceed a value of about 150. For divergence angles too much greater than 15 deg, the flow will separate from the nozzle walls short of the exit even though the nozzle is operating at design altitude $P_a = P_e$. Conversely, for a given divergence angle, the flow will separate if the nozzle back-pressure ratio P_a/P_e is too high ($P_a/P_e > 1$ when a nozzle is operating at an altitude lower than the design altitude). When separation occurs, oblique shock wave A (Fig. 3.17) is located inside the nozzle, and the gas flow is contained within the jet boundary or slip line shown. Figure 3.17 depicts the real flow situation that occurs (other than under ideal laboratory conditions) in place of normal shocks near the exit section as shown in Fig. 2.37.

Summerfield has established a criterion for judging whether or not separation is likely to occur in the exit section of a conical nozzle.[20] The criterion is based on

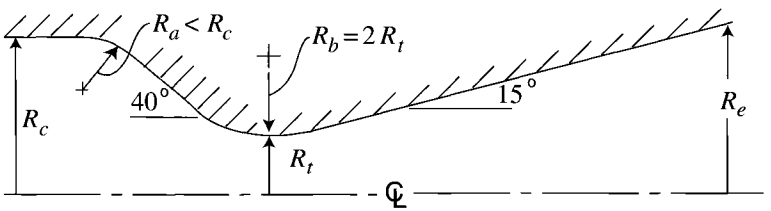

Fig. 3.16 Conical convergent-divergent nozzle.

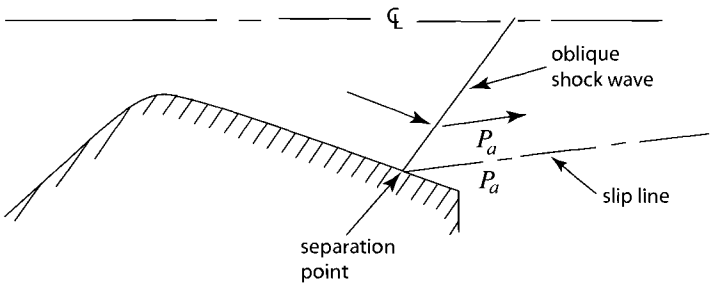

Fig. 3.17 Separation in overexpanded nozzle.

an accumulation of experimental separation data points from many sources. The experimental data give the pressure ratios P_a/P_{we} (P_{we} = wall pressure at exit = P_e for 15-deg conical nozzle) that produced flow separation in tests of 15-deg conical nozzles for various nozzle-pressure ratios. The data points are scattered throughout the cross-hatched region of Fig. 3.18. The Summerfield criterion states that for back-pressure ratios greater than 2.5, separation is likely to occur in the exit of a 15-deg conical nozzle for nozzle-pressure ratios in excess of 20. Current data on large rocket nozzles indicate that the critical back-pressure ratio for these large nozzles is 3.5. This increase in the permissible back-pressure ratio for no separation is to be expected as nozzle sizes increase because the boundary layer forms a smaller percentage of the total flow for larger nozzles. Using this modified Summerfield criterion value of 3.5, it should be noted that

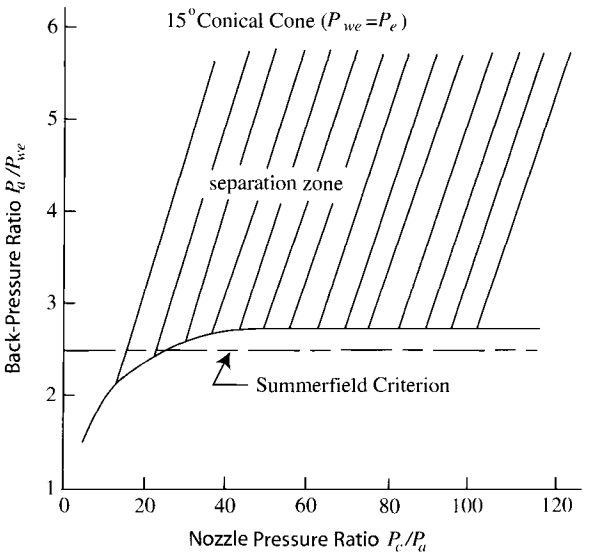

Fig. 3.18 Summerfield separation criterion.

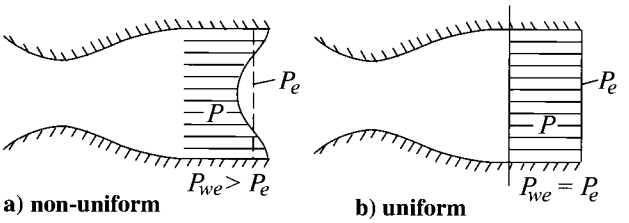

Fig. 3.19 Pressure profile at nozzle exit.

for large rocket nozzles, separation occurs when $P_a > 3.5\ P_{we}$. For a 15-deg conical nozzle, $P_{we} = P_e$ because the stream properties at the exit section are essentially uniform at the values determined by one-dimensional flow analysis. In some nozzles, the streams are not uniform across the exit section and $P_{we} > P_e$ (Fig. 3.19). Separation will occur sooner (at lower values of P_a) in a conical nozzle than in those of the same area ratio for which $P_{we} > P_e$.

3.4.2 Bell Nozzle

The bell-shaped nozzle of the Atlas sustainer engine (shown in Fig. 3.20) is designed to reduce the thrust and length disadvantages of a conical nozzle. To reduce length, a bell-shaped nozzle employs a high divergence angle at the throat with a very rapid expansion of the gases from the throat. The flow is then turned rather abruptly back toward the axial direction. The comparative lengths of a bell-shaped (L_B) and a conical (L_C) nozzle having the same expansion ratio are indicated in Fig. 3.20. The bell-shaped contour is used on several current engines. The bell-shaped nozzle on the H-1 Saturn 1B engine has a length 20%

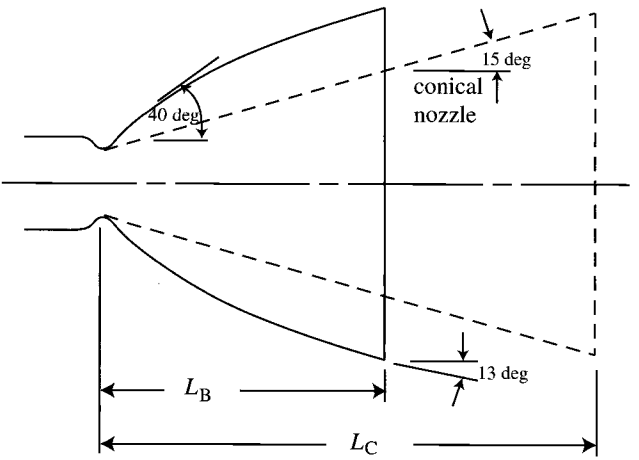

Fig. 3.20 Bell-shaped nozzle $A_e/A_t = 25$ (Atlas sustainer engine).

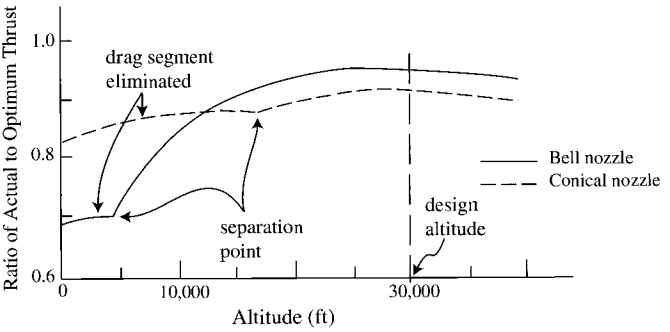

Fig. 3.21 Ratio of actual-to-optimum thrust for bell-shaped and conical nozzles vs altitude (pressure ratio).

less than the length that would be required for a 15-deg conical nozzle with the same 8:1 area ratio.

3.4.3 Free-Expansion (Plug) Nozzle

Figure 3.21 depicts the performance loss of conventional convergent-divergent (C-D) nozzles at off-design pressure ratios. To avoid the large penalties (Fig. 3.21) at liftoff pressure ratios, relatively low-area-ratio nozzles must be used. Note that high-area-ratio nozzles, however, improve performance at altitude. (Atlas booster—low-altitude operation—area ratio is 8:1. Atlas sustainer—high-altitude operation—area ratio is 25:1). Use of a high-altitude nozzle, such as the Atlas sustainer, at liftoff incurs a large performance degradation. To avoid such losses at off-design operation, a rocket nozzle with an adjustable area ratio that provides optimum expansion at each ascending altitude is needed. Obviously, a variable area C-D nozzle is not feasible because of hardware considerations. It is possible, however, to design a nozzle so that the expanding flow is not bound by immovable solid walls. In such free-expansion nozzles (Figs. 3.22 and 3.23), the expanding flow is bound by a solid surface and a free-to-move slip-line expansion surface. The adjustable slip-line boundary, in effect, produces a variable area ratio nozzle that accommodates itself to changing nozzle pressure ratios. Free-expansion nozzles, therefore, tend to operate at optimum expansion, with the ratio of thrust-to-optimum-thrust being quite insensitive to altitude variations (Fig. 3.24). The free-expansion nozzles shown in Fig. 3.22 have been dubbed "plug nozzles." The manner in which the flow adjusts to varying back-pressures for the two types of plug nozzles of Fig. 3.22 is shown in Figs. 3.25 and 3.26.

Note the performance gain of a free-expansion-type nozzle in the test data curves of Fig. 3.24 (ratio of actual thrust to optimum thrust plotted versus altitude). The improved performance of the free-expansion type of nozzle over the bell nozzle at lower off-design altitudes is evident. The absence of large thrust

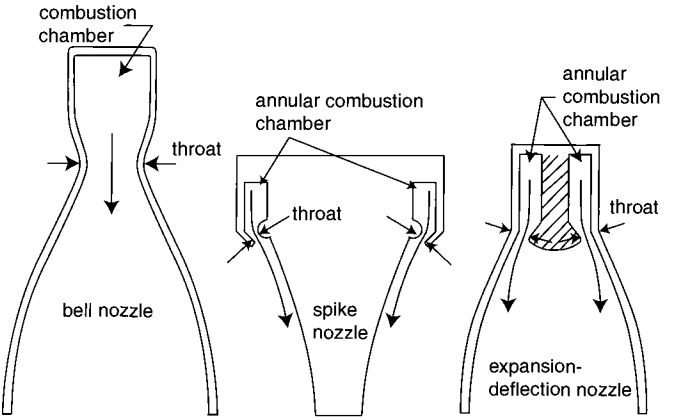

Fig. 3.22 Bounded and free-expansion nozzles.

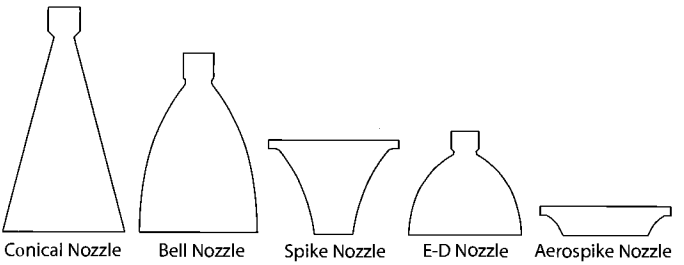

Fig. 3.23 Nozzle type and size comparison.

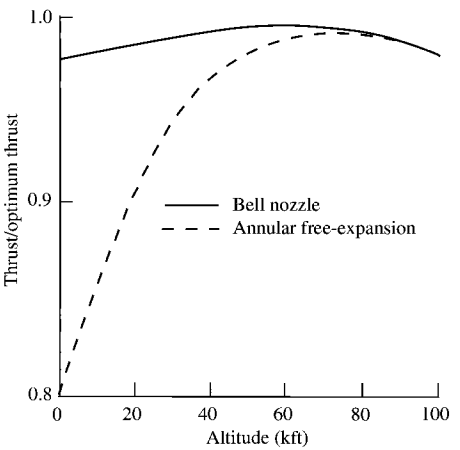

Fig. 3.24 Performance comparison of a bell nozzle and a free-expansion nozzle.

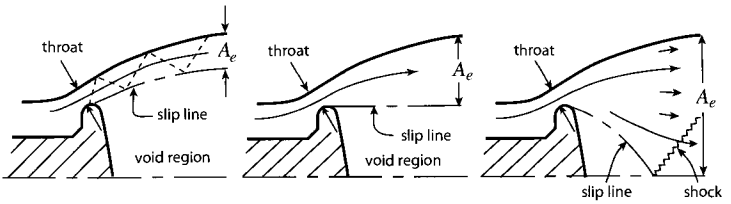

a) Low altitude **b) Intermediate altitude** **c) High altitude**

Fig. 3.25 Exhaust flow pattern from expansion-deflection (ED) plug nozzle.

losses at lower altitudes suggests that a free-expansion-type nozzle would be particularly suited for use in both boosters or in single-stage ballistic missiles.

3.5 Parameters for Chemical Rockets

The nozzle mass flow, ideal thrust equation, characteristic velocity, exit velocity, and area ratio for isentropic flow follow from the relations developed in Chapter 2. The purpose here is simply to write expressions for these quantities in forms that are particularly useful for substitution into the ideal chemical rocket-thrust coefficient equation to be developed later in this section. After deriving the mass flow and ideal thrust equations desired, the characteristic velocity C^* will be introduced. The expressions for mass flow rate, ideal thrust, C^*, V_e, and A_e/A_t will be written in terms of quantities relating to rocket nozzle hardware and gross parameters, such as chamber pressure and temperature. To identify the flow properties more closely with the physical hardware, the following notations will be adopted: the subscript 'c' will denote combustion chamber; thus, P_c and T_c will designate the combustion chamber temperature and pressure, which we will assume corresponds to the total pressure and temperature of the ideal flow; the nozzle throat conditions will be represented by a subscript 't' and exit section quantities by a subscript 'e.' Because the flow in the ideal rocket nozzle is isentropic, with sonic flow at the throat, we have $A_t = A^*$, $P_t = P^*$, etc.

3.5.1 Rocket Nozzle Mass Flow

The mass flow through a nozzle is conveniently determined by applying the mass flow parameter equation at the nozzle throat where $M_t = 1.0$. We have, from Eq. (2.76), using the notation just introduced,

$$\frac{\dot{m}\sqrt{T_c}}{P_c A_t} = \frac{(1)\sqrt{\gamma g_c/R}}{\left\{1 + \dfrac{\gamma - 1}{2}(1)^2\right\}^{\frac{\gamma+1}{2(\gamma-1)}}}$$

$$\frac{\dot{m}\sqrt{T_c}}{P_c A_t} = \sqrt{\frac{g_c}{R}\gamma\left\{\frac{\gamma+1}{2}\right\}^{-\frac{\gamma+1}{\gamma-1}}} = \frac{\Gamma}{\sqrt{R/g_c}} \tag{3.34}$$

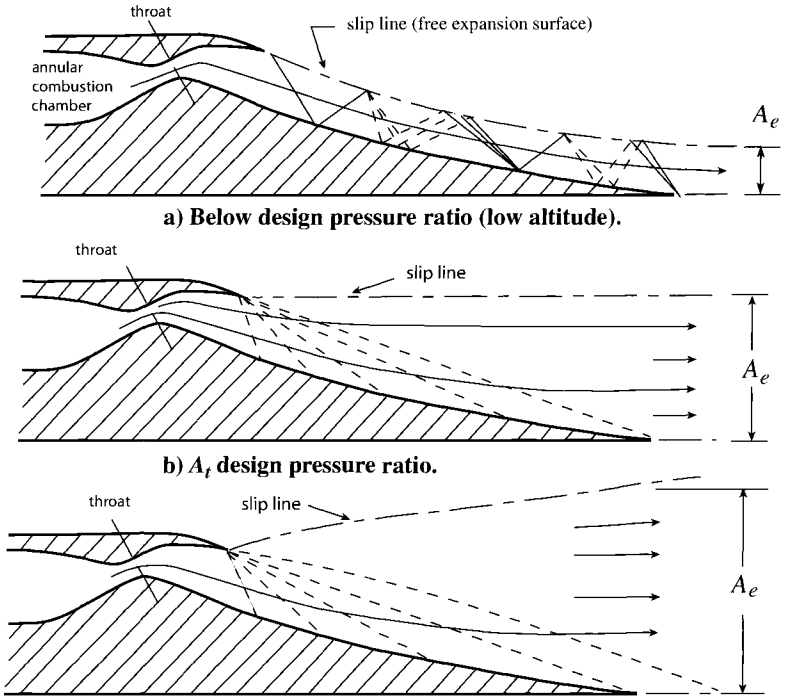

Fig. 3.26 Exhaust flow pattern from annular free-expansion nozzle.

where

$$\Gamma = \sqrt{\frac{\gamma}{\left\{\frac{\gamma+1}{2}\right\}^{\frac{\gamma+1}{\gamma-1}}}} \tag{3.35}$$

We introduce Γ because it is simpler to write than the square root of many exponential terms involving γ. Γ is a function of the combustion gases' specific heat ratio alone and is given in Table 3.10 for a range of γ values. The ratio Γevaluated for air should give the value of Fig. 2.20 at $M = 1.0$ and $\gamma = 1.4$.

To illustrate the use of Table 3.10 and the little-but-ever-with-us matter of units, let us evaluate $\Gamma/\sqrt{R/g_c}$ for $\gamma = 1.4$ and $R = 53.34$ ft-lbf/lbm-°R:

$$\frac{\dot{m}\sqrt{T_c}}{P_c A_t} = \frac{\Gamma}{\sqrt{R/g_c}} = \frac{0.6847}{\sqrt{53.34/32.174}} = 0.5318 \frac{\text{lbm-}\sqrt{^\circ R}}{\text{lbf-s}}$$

This value agrees with the GASTAB software.

Table 3.10 Γ tabulated vs γ

γ	Γ	γ	Γ	γ	Γ
1.14	0.6366	1.21	0.6505	1.28	0.6636
1.15	0.6386	1.22	0.6524	1.29	0.6654
1.16	0.6406	1.23	0.6543	1.30	0.6673
1.17	0.6426	1.24	0.6562	1.31	0.6691
1.18	0.6446	1.25	0.6581	1.32	0.6726
1.19	0.6466	1.26	0.6599	1.33	0.6779
1.20	0.6485	1.27	0.6618	1.34	0.6847

Solving Eq. (3.34) for the mass flow rate, we obtain the following simple expression for rocket nozzle mass flow:

$$\dot{m} = P_c A_t g_c \frac{\Gamma}{\sqrt{R g_c T_c}} \tag{3.36}$$

The mass flow rate is seen to be determined by the nozzle throat area, the combustion chamber pressure, and the quantity $(\Gamma/\sqrt{Rg_cT_c})$. The latter is determined by the combustion gas temperature T_c and the combustion gases' characteristics, γ and R.

Example 3.5

Determine the mass flow rate of a gas with a molecular weight of 18 and $\gamma = 1.25$ through a choked throat area of 2 ft^2 from a combustion chamber whose pressure is 2000 psia and temperature is 3000°R. From Eq. (3.35) or Table 3.10, $\Gamma = 0.6581$. For the gas, $R = \mathscr{R}/\mathscr{M} = 1545/18 = 85.83$ ft-lbf/(lbm-°R). Using Eq. (3.36), we have

$$\dot{m} = P_c A_t g_c \frac{\Gamma}{\sqrt{R g_c T_c}} = \frac{2000 \times 2 \times 144 \times 32.174 \times 0.6581}{\sqrt{85.83 \times 32.174 \times 3000}} = 4237 \text{ lbm/s}$$

3.5.2 Ideal Thrust Equation

The ideal thrust is given by Eq. (3.1). Using the one-dimensional isentropic relationship of Chapter 2 for V_e, we get

$$V_e = \sqrt{\frac{2\gamma}{\gamma - 1} R g_c T_c \left\{ 1 - \left(\frac{P_e}{P_c} \right)^{\frac{\gamma - 1}{\gamma}} \right\}}$$

Combining this equation for V_e and Eq. (3.36) for the mass flow rate with Eq. (3.1), we get the following ideal thrust equation in terms of areas, pressures, and γ:

$$F_i = P_c A_t \left\{ \Gamma \sqrt{\frac{2\gamma}{\gamma - 1}\left[1 - \left(\frac{P_e}{P_c}\right)^{\frac{\gamma-1}{\gamma}}\right]} + \left(\frac{P_e}{P_c} - \frac{P_a}{P_c}\right)\frac{A_e}{A_t} \right\} \tag{3.37}$$

3.5.3 Characteristic Velocity, C^*

The quantity $(\sqrt{Rg_c T_c}/\Gamma)$ of Eq. (3.36) has the dimensions of velocity, and as just noted, its value is determined by the combustion gas temperature T_c and the combustion gases' characteristics, γ and R. For a given propellant, therefore, the quantity $(\sqrt{Rg_c T_c}/\Gamma)$ is a characteristic of the reaction process of the propellant because the propellant's combustion process will establish the flame temperature T_c and the composition of the gas mixture making up the products of combustion.

The composition of the combustion gases in turn establishes γ and the molecular weight $\mathscr{M}$ (hence R, which equals $\mathscr{R}_u/\mathscr{M}$, where $\mathscr{R}_u$ is the universal gas constant). This quantity, which has the dimensions of velocity and a value characterized by the propellant combustion process, is called the characteristic velocity C^*. (The superscript star bears no relation to the star notation used for sonic flow properties.) Thus, by definition

$$C^* = \frac{\sqrt{Rg_c T_c}}{\Gamma} \tag{3.38}$$

The characteristic velocity can be determined theoretically by the methods of thermochemistry.[14] This theoretical value can be compared with an experimentally determined value of C^* to evaluate the actual combustion process against the "theoretical" combustion process. Experimental values of C^* can be obtained in a rocket motor test by measuring the propellant mass flow rate, the chamber pressure P_c, and the nozzle throat area A_t. These data and Eq. (3.36) give the experimental value C_x^*. Thus,

Experimental:

$$C_x^* = \frac{P_c A_t}{\dot{m}/g_c}$$

with P_c, A_t, and m obtained from measured data. Also, from Eq. (3.38) defining C_i^*

Theoretical:

$$C_i^* = \frac{\sqrt{Rg_c T_c}}{\Gamma}$$

with R, T_c, and Γ obtained from thermochemistry.

A well-designed combustion chamber should give a value of C_x^* in excess of 90% of the theoretical value computed by thermochemical means and Eq. (3.38). An experimental value of C_x^* less than 0.9 of the theoretical value would be evidence of a poorly designed combustion chamber or injector.

With present-day propellants, C^* ranges from 3000 to 7000 ft/s. The value of C^* for the design point operation of the Atlas sustainer rocket motor is 5440 ft/s.

3.5.4 Nozzle Exit Velocity, V_e

The expansion flow process through an ideal nozzle from a pressure P_c to P_e is shown on the temperature-entropy diagram of Fig. 3.27. The kinetic energy imparted to the expanding gas is proportional to the vertical distance indicated. There is also depicted the maximum possible kinetic energy that could be delivered to the expanding gas. This maximum corresponds to an expansion to zero absolute temperature.

It is seen from the diagram that $V_e^2/(2c_p) = T_c - T_e$. Using this and the perfect gas relations accompanying the T-s diagram of Fig. 3.27, we obtain

$$V_e = \sqrt{\frac{2\gamma}{\gamma - 1}\frac{\mathcal{R}}{\mathcal{M}} g_c T_c \left\{1 - \left(\frac{P_e}{P_c}\right)^{\frac{\gamma-1}{\gamma}}\right\}} \tag{3.39}$$

The ratio of the exit velocity to the maximum possible exit velocity is

$$\frac{V_e}{V_{\max}} = \sqrt{1 - \left(\frac{P_e}{P_c}\right)^{\frac{\gamma-1}{\gamma}}} \tag{3.40}$$

Because a high exit velocity means, for a given nozzle mass flow, a large momentum flux and, hence, thrust, let us examine the terms of Eq. (3.39) upon which V_e depends. These variables are 1) the pressure ratio P_c/P_e, 2) the chamber temperature T_c, and 3) the molecular weight $\mathcal{M}$.

Varying the specific heat ratio γ is of little practical use and will not be considered. Before discussing these factors, let us first note that for chemically

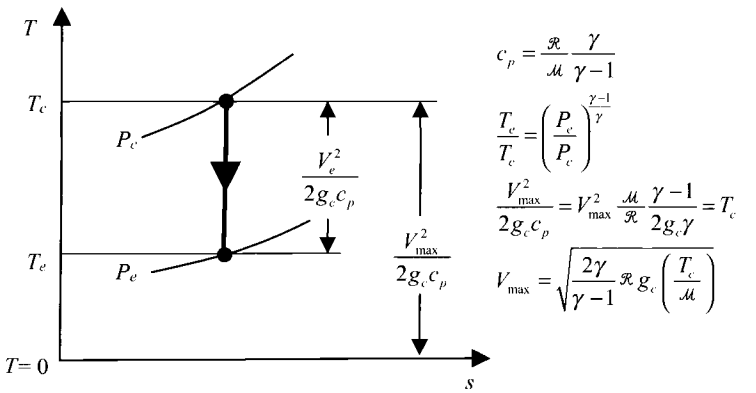

Fig. 3.27 Nozzle expansion process.

propelled rockets, the original source of kinetic energy V_e^2 is the ejected material itself, i.e., the propellant's chemical energy. For chemical rockets, therefore, the choice of propellant is fixed by the selection of fuel and oxidizer. If, on the other hand, the rocket combustion chamber is replaced with a nuclear reactor, then the reactor's fuel becomes the original source of the propellant's kinetic energy. In this case, the energy is supplied by a source independent of the propellant, and one can choose a propellant without consideration of its chemical energy. This is pointed out here because T_c and $\mathscr{M}$ are somewhat interdependent for a chemical rocket but can be completely independent in other cases.

Allowance can be made for these different situations in considering the influence of T_c and $\mathscr{M}$ on V_e in the following:

1) *Pressure Ratio* P_c/P_e. The pressure ratio determines what fraction of the maximum possible velocity is ideally attained. As P_c/P_e increases, V_e increases very rapidly (Fig. 3.28) up to a pressure ratio of 10. Above this value of P_c/P_e, the velocity increases less rapidly with pressure ratio. Increasing chamber pressure is thus seen to have a favorable influence on V_e. The favorable influence is limited, however, because a higher P_c means increased structural weight requirements and, for liquid chemical propellant rockets, increased propellant feed system weight. Note also that as P_c/P_e increases, the nozzle-area ratio must increase. The Atlas booster ($A_e/A_t = 8$) and sustainer ($A_e/A_t = 25$) operate with a pressure ratio (P_c/P_e) of 60 and 250, respectively.

2) *Chamber Temperature* T_c. The exit velocity V_e increases as the square root of the chamber temperature T_c. The upper limit on T_c is fixed by either structural (in the case of a nonchemical nuclear rocket) or chemical considerations. Usually, in a liquid chemical rocket, cooling alleviates the

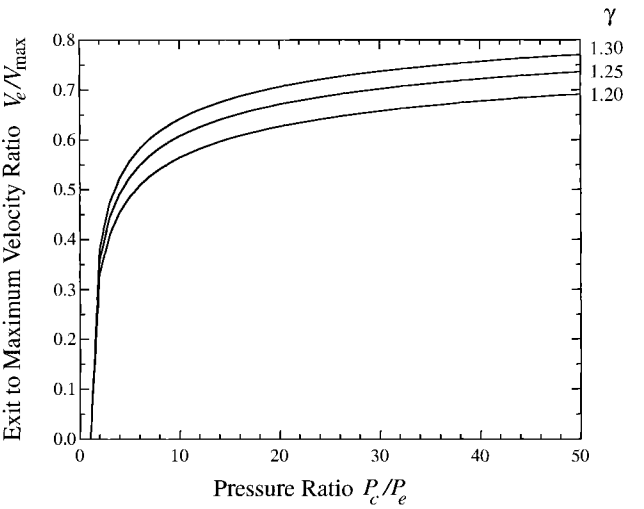

Fig. 3.28 Fraction of maximum velocity vs pressure ratio.

structural limitation so that T_c is limited by chemical considerations. From a chemical point of view, it would appear that fuels with greater chemical energy will give an increasingly higher temperature T_c. This is true up to a temperature where dissociation of the combustion products—CO_2 dissociating into C and O_2 for example—occur and absorb energy that would otherwise be available for increasing T_c. Thus we find that for the best fuels, dissociation sets an upper temperature limit of about 6000°R.

3) *Molecular Weight* $\mathscr{M}$. Since V_e varies inversely as the square root of $\mathscr{M}$, propellants with a low molecular weight are preferable. For chemical rockets, the molecular weight of the propellant is determined by the fuel and oxidizer and is on the order of 20. In a nuclear rocket, one has a freer choice of a propellant than in a chemical rocket, and hydrogen with a molecular weight of 2 can be used. A nuclear rocket, using H_2 for a propellant and having the same temperature T_c and pressure ratio P_c/P_e as a chemical rocket with $\mathscr{M} = 20$, would have a higher V_e factor $\sqrt{20/2} = \sqrt{10}$. This factor is approximately equal to the ratio of the exit velocities of the LOX-RP and the nuclear-H2 propulsion systems of Table 3.2. This is to be expected since the LOX-RP and the nuclear-H_2 systems each encounter the same structural limitations on T_c and P_c/P_e, so that the main difference in V_e between the two is due to the lower molecular weight of the nuclear system's propellant.

4) *Simultaneous Effect of Combustion Temperature and Molecular Weight on* V_e. Up to this point, we have considered the combustion temperature and molecular weight effects on exit velocity independent of each other. For a given fuel-oxidizer combination in a chemical rocket, the combustion temperature T_c and the molecular weight $\mathscr{M}$ of the propellant are interdependent. They vary simultaneously with mixture ratio and chamber pressure. Consequently, the influence of these two variables on V_e must, in this case, be considered together as the mixture ratio is varied for a given chamber pressure. Figure 3.29 shows the variation of T_c and $\mathscr{M}$, along with V_e, for a chamber pressure of 300 psia and a pressure ratio of $P_c/P_e = 20.4$ for a LOX-gasoline fuel combination. As the mixture ratio is increased from 1.5, we observe that the combustion temperature and molecular weight each increase. The former increases more rapidly initially so that the net effect of the ratio $T_c/\mathscr{M}$ on the velocity V_e [Eq. (3.39)] is to increase V_e as shown. As the mixture ratio is increased beyond 2.5, the molecular weight increases more rapidly than the temperature, thus producing lower values of the ratio $T_c/\mathscr{M}$ and, hence, V_e. The optimum mixture ratio for the LOX-gasoline system is, therefore, a value of 2.5. This compares with a stochiometric mixture ratio of 3.5 for LOX-gasoline. The mixture ratio of the LOX-RP-l combination used in the Atlas booster engine (YLR89-NA-7 model) is 2.38.

The curves of Fig. 3 .29 are for one chamber pressure. If a similar set of curves were drawn for a higher chamber pressure, the same general results would be obtained except that V_e would be higher due to the favorable effect of a higher pressure in reducing dissociation of the combustion products. Increasing the chamber pressure to obtain higher V_e, however, produces the unfavorable effect of increasing dead weight because of the higher stress levels introduced

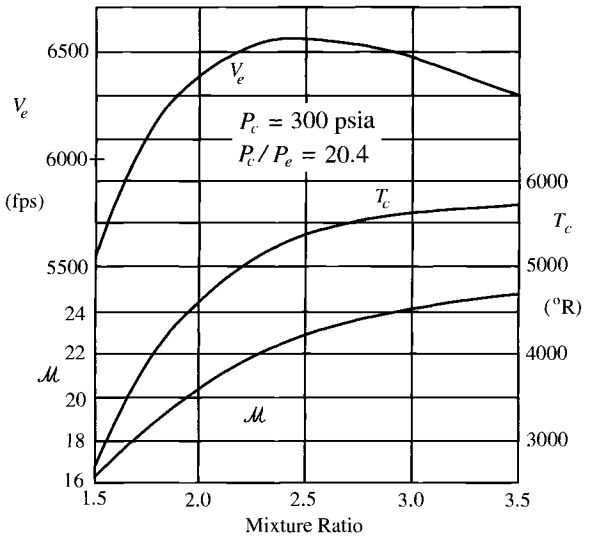

Fig. 3.29 LOX-gasoline performance vs mixture ratio.

and the added fuel feed system pressure requirements. In any particular application, the operating chamber pressure selected must be a compromise of the several interrelated factors that chamber pressure effects.

3.5.5 Area Ratio and Velocity Ratio in Terms of the Pressure Ratio

The isentropic area ratio A/A^*, calculated in program GASTAB and written as a function of the Mach number in Eq. (2.77), can be used to obtain the nozzle area ratio A_e/A_t when the exit Mach number is known. It is useful in rocket performance work to have the nozzle area expansion ratio A_e/A_t expressed in terms of the ratio of the rocket chamber pressure to the exit section pressure P_c/P_e for isentropic flow. This relation can be obtained rather directly by use of the mass flow parameter given in terms of $\Gamma/\sqrt{R/g_c}$ [Eq. (3.34)] and pressure ratio [Eq. (3.2)]. Thus with $P_t = P_c$ and $T_t = T_c$, we have from Eq. (3.34)

$$\frac{\dot{m}\sqrt{T_c}}{P_c A_t} = \frac{\Gamma}{\sqrt{R/g_c}}$$

Writing Eq. (3.2) for the exit station ($P = P_e$) and rearranging gives

$$\frac{\dot{m}\sqrt{T_c}}{P_c A_e} = \sqrt{\frac{2g_c}{R}\left(\frac{\gamma}{\gamma-1}\right)\left[\left(\frac{P_e}{P_c}\right)^{\frac{2}{\gamma}} - \left(\frac{P_e}{P_c}\right)^{\frac{\gamma+1}{\gamma}}\right]}$$

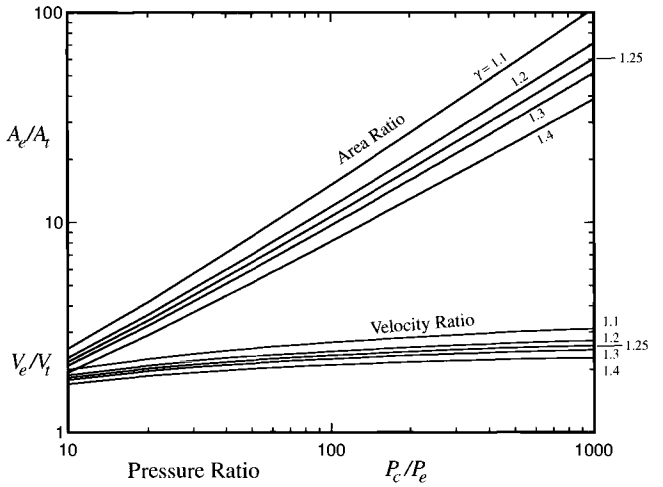

Fig. 3.30 Area and velocity ratios vs pressure ratio.

Dividing Eq. (3.34) by the preceding equation gives the desired expression for the area ratio A_e/A_t [Eq. (3.35)]:

$$\frac{A_e}{A_t} = \frac{\Gamma}{\sqrt{\dfrac{2\gamma}{\gamma-1}\left[\left(\dfrac{P_e}{P_c}\right)^{\frac{2}{\gamma}} - \left(\dfrac{P_e}{P_c}\right)^{\frac{\gamma+1}{\gamma}}\right]}} \tag{3.41}$$

Similarly, the ratio of the velocity at the exit, V_e, to the velocity at the throat, V_t, can be expressed as

$$\frac{V_e}{V_t} = \sqrt{\frac{\gamma+1}{\gamma-1}\left[1 - \left(\frac{P_e}{P_c}\right)^{\frac{\gamma-1}{\gamma}}\right]} \tag{3.42}$$

Equations (3.41) and (3.42) are plotted for several values of γ vs P_c/P_e on Fig. 3.30 as A_e/A_t and as V_e/V_t, respectively. Note that an area ratio (A_e/A_t) of 50 is required to obtain a value of two for V_e/V_t with $\gamma = 1.4$.

3.5.6 Thrust Coefficient

The thrust coefficient is defined as the thrust F divided by the product of the chamber pressure and throat area, P_cA_t, or

$$C_F \equiv \frac{F}{P_cA_t} \tag{3.43}$$

Why use thrust coefficient in place of thrust?

1) It is a dimensionless quantity.
2) Its numerical values have a convenient size that fall in range 0.6–2.2.
3) It provides a figure of merit that is independent of size of rocket and forms a common basis with which to compare different-sized rockets.

3.5.7 Ideal Thrust Coefficient, C_{Fi}

The proportionality factor between F_i and $P_c A_t$ is called ideal thrust coefficient. From Eqs. (3.37) and (3.43) we have

$$C_{Fi} = \Gamma \sqrt{\frac{2\gamma}{\gamma - 1}\left[1 - \left(\frac{P_e}{P_c}\right)^{\frac{\gamma-1}{\gamma}}\right]} + \left(\frac{P_e}{P_c} - \frac{P_a}{P_c}\right)\frac{A_e}{A_t} \tag{3.44}$$

C_{Fi} is a function of A_e/A_t and P_c/P_a—the nozzle area and pressure ratios—for given γ. Note that A_e/A_t determines P_e/P_c through Eq. (3.41). Using Eqs. (3.44) and (3.41), one can express the maximum value of the ideal thrust coefficient as

$$(C_{Fi})_{\max} = \Gamma \sqrt{\frac{2\gamma}{\gamma - 1}} \tag{3.45}$$

3.5.8 Optimum Thrust Coefficient, $(C_{Fi})_{opt}$

For optimum ideal thrust, $P_e = P_a$ and Eq. (3.44) gives

$$(C_{Fi})_{\text{opt}} = \Gamma \sqrt{\frac{2\gamma}{\gamma - 1}\left[1 - \left(\frac{P_e}{P_c}\right)^{\frac{\gamma-1}{\gamma}}\right]} \tag{3.46}$$

Note: It can be shown that

$$\frac{A_e}{A_t} = \frac{\gamma - 1}{2\gamma}\left(\frac{P_e}{P_c}\right)^{\frac{1}{\gamma}} \frac{(C_{Fi})_{\text{opt}}}{1 - \left(\frac{P_e}{P_c}\right)^{\frac{\gamma-1}{\gamma}}} \tag{3.47}$$

3.5.9 Vacuum Thrust Coefficient, $(C_{Fi})_{vac}$

For vacuum, $P_a = 0$ and Eqs. (3.44) and (3.46) give

$$(C_{Fi})_{\text{vac}} = (C_{Fi})_{\text{opt}} + \frac{P_e}{P_c}\frac{A_e}{A_t} \tag{3.48}$$

or

$$(C_{Fi})_{\text{vac}} = C_{Fi} + \frac{P_a}{P_c}\frac{A_e}{A_t} \tag{3.49}$$

3.5.10 Graphs for Determining Ideal Thrust Coefficient

Equation (3.44) can be solved conveniently by use of graphs. In Fig. 3.31 $(C_{Fi})_{\text{vac}}$ is plotted vs γ and nozzle area ratio ε. Figure 3.30, which gives a plot of nozzle area ratio and velocity ratio vs P_c/P_e, is handy in computational work when the area ratio or P_c/P_e is known and the value of the other is required. Figures 3.32–3.35 present C_{Fi} for various conditions. Figure 3.32 is a plot of $(C_{Fi})_{\text{opt}}$ vs nozzle pressure ratio with optimum expansion. The dashed curves in the lower right of Fig. 3.33 ($\gamma = 1.2$), Fig. 3.34 ($\gamma = 1.25$), and Fig. 3.35 ($\gamma = 1.3$) are plots of (C_{Fi}) with flow separation (Summerfield criterion for separation of $P_a > 3.5\ P_{\text{we}}$). The remaining curves present Eq. (3.44) for various values of P_c/P_a.

Example 3.6

We can illustrate the use of the graph of Fig. 3.31 with an example. Let us find C_{Fi} for a rocket at 100,000-ft altitude with an area ratio of 25, $\gamma = 1.29$, and a chamber pressure $P_c = 500$ psia. Because the value of γ is not one of the specific values plotted in Figs. 3.30 and 3.32–3.35, use of Fig. 3.31 presents a convenient

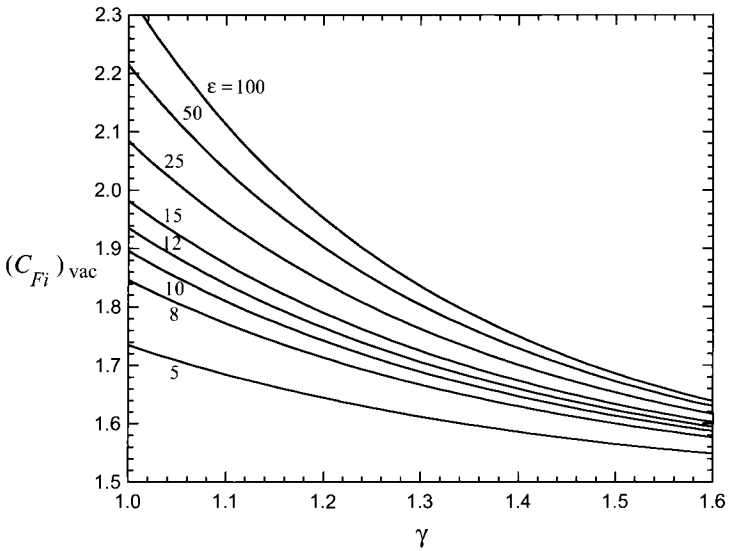

Fig. 3.31 Vacuum thrust coefficient, $(C_{Fi})_{\text{vac}}$.

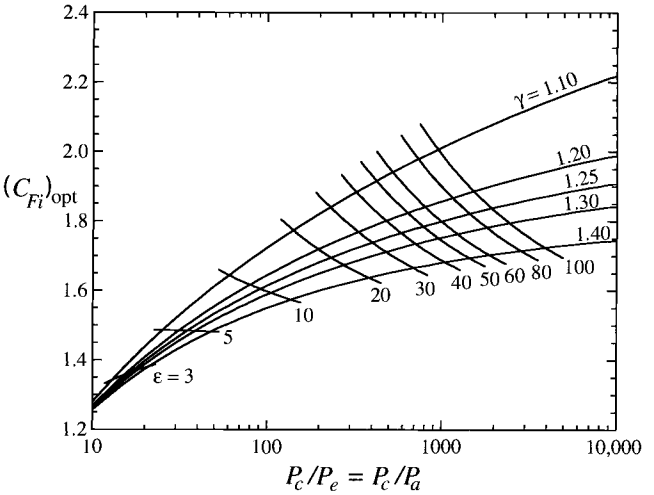

Fig. 3.32 Optimum thrust coefficient vs pressure ratio.

way of finding C_{Fi} without interpolation. First, we note that Eq. (3.45) can be written as

$$C_{Fi} = (C_{Fi})_{\text{vac}} - \frac{P_a}{P_c}\frac{A_e}{A_t}$$

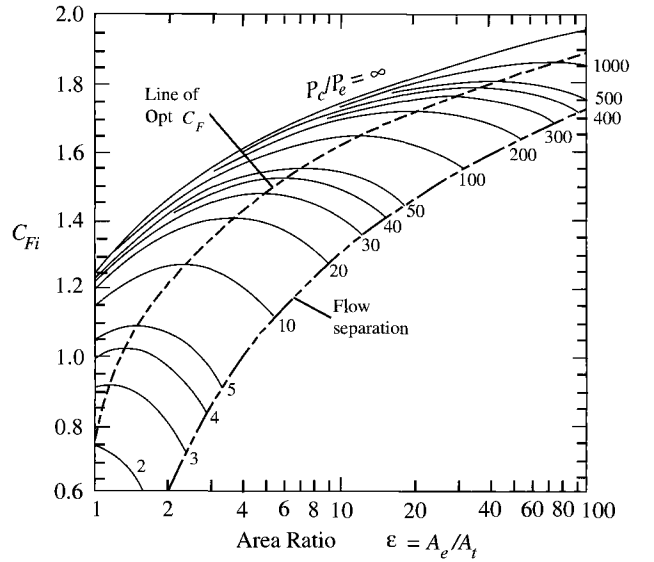

Fig. 3.33 Ideal thrust coefficient vs area ratio ($\gamma = 1.2$).

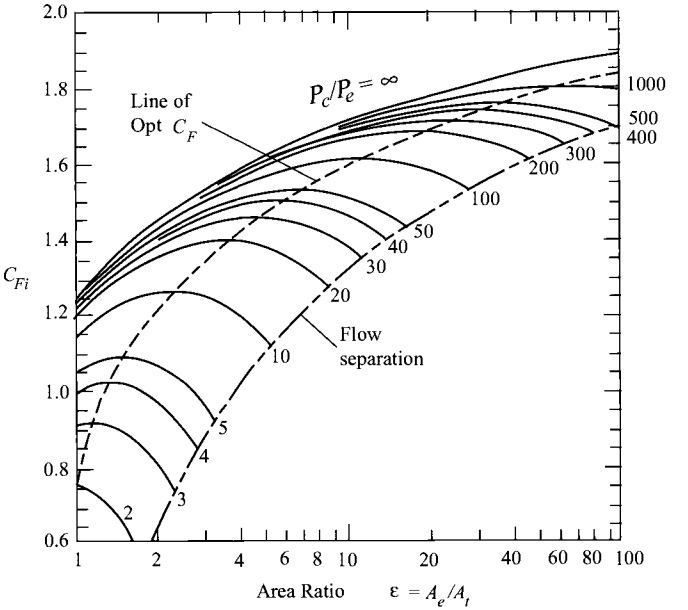

Fig. 3.34 Ideal thrust coefficient vs area ratio ($\gamma = 1.25$).

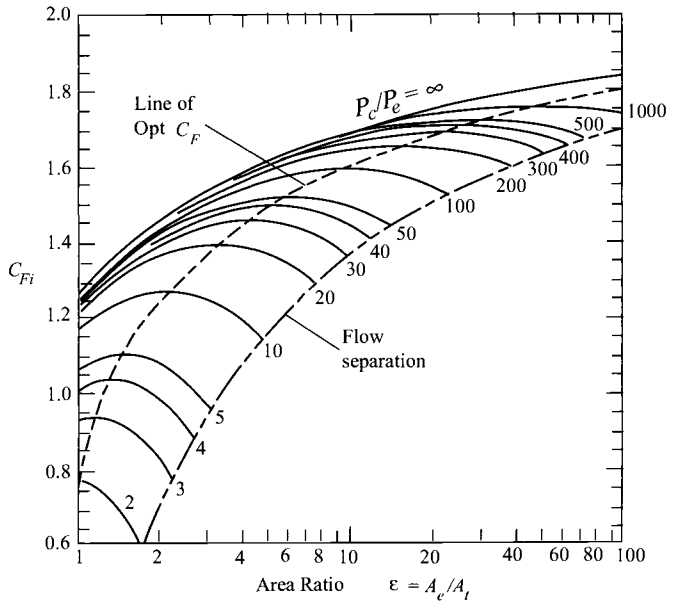

Fig. 3.35 Ideal thrust coefficient vs area ratio ($\gamma = 1.3$).

or

$$C_{Fi} = (C_{Fi})_{\text{vac}} - \Delta C_F \tag{3.50a}$$

where

$$\Delta C_F = \frac{P_a}{P_c}\frac{A_e}{A_t} \tag{3.50b}$$

Thus C_{Fi} can easily be found by getting the value of $(C_{Fi})_{\text{vac}}$ from Fig. 3.31 and calculating the value of ΔC_F provided that the nozzle flow is not separated. From the standard atmosphere data in Appendix A, the atmospheric pressure P_a at 100,000 ft is 23.28 lbf/ft^2 (2116 × 0.0110) or 0.162 psia. Using the given value for P_c and this value of P_a gives a value of 3086 for the ratio P_c/P_a. A quick check of Figs. 3.34 and 3.35, with this value of P_c/P_a and the given value for nozzle area ratio ε, shows that the nozzle is operating underexpanded, and flow is not separated in the nozzle. Thus Fig. 3.31 and Eqs. (3.50a) and (3.50b) can be used to determine the ideal thrust coefficient. We obtain $(C_{Fi})_{\text{vac}} = 1.770$ from Fig. 3.31 corresponding to $\gamma = 1.29$ and $\varepsilon = 25$. Using the value of P_a determined in the preceding and the given data for P_c and ε in Eq. (3.50b) gives

$$\Delta C_F = \frac{P_a}{P_c}\frac{P_e}{A_t} = \frac{0.162}{500}25 = 0.008$$

Thus

$$C_{Fi} = (C_{Fi})_{\text{vac}} - \Delta C_F = 1.770 - 0.008 = 1.762$$

3.5.11 Relationship Between C, C*, and C_{Fi}

Noting that from Eqs. (3.36) and (3.38), we can write

$$P_c A_t = \dot{m}C^*/g_c \tag{i}$$

from Eqs. (3.5) and (3.43), we have

$$C_{Fi} = \frac{F_i}{P_c A_t} = \frac{\dot{m}C/g_c}{P_c A_t} \tag{ii}$$

Substituting Eq. (i) into Eq. (ii) and solving for the effective exhaust velocity C gives

$$C = C_{Fi}C^* \tag{3.51}$$

This equation shows that the effective exhaust velocity C can be expressed as the product of the ideal thrust coefficient (dependent primarily on the nozzle area and pressure ratios) times the characteristic velocity (dependent on thermochemistry).

Example 3.7

The space shuttle main engine (SSME) operates for up to 520 s in one mission at altitudes over 100 miles. The nozzle expansion ratio ε is 77:1, and the inside exit diameter is 7.54 ft. Assume a calorically perfect gas with the following properties: $\gamma = 1.25$, $P_c = 3000$ psia, $T_c = 6890°$F, and $R = 112$ ft-lbf/(lbm-°R).

We want to calculate the following:

1) Characteristic velocity C^*.
2) Mass flow rate of gases through the nozzle.
3) Mach number at exit M_e.
4) Altitude that nozzle is "on-design."
5) Altitude that flow in nozzle is just separated (assume separation occurs when $P_a > 3.5\ P_{we}$).
6) Ideal thrust coefficient C_{Fi} and the ideal thrust F_i in 5000-ft increments from sea level to 40,000 ft; in 10,000-ft increments from 40,000 to 100,000 ft; and at vacuum.
7) $(I_{sp})_{vac}$ for the engine.
8) Actual exhaust velocity V_e and effective exhaust velocity C at sea level.

Solution: We assume isentropic flow of a perfect gas with constant specific heats.

a) Characteristic velocity C.*

$$C^* = \sqrt{Rg_cT_c}/\Gamma$$

where $\Gamma = 0.6581$ for $\gamma = 1.25$ and $T_c = 7350°$R. Thus

$$C^* = \sqrt{112 \times 32.174 \times 7350}/0.6581 = 7820 \text{ ft/s}$$

b) Mass flow rate.

$$\dot{m} = P_cA_tg_c/C^*$$

where

$$A_e = \frac{\pi D_e^2}{4} = \frac{\pi \times 7.54^2}{4} = 44.65 \text{ ft}^2$$

Then

$$A_t = \frac{A_e}{\varepsilon} = \frac{44.65}{77}144 = 83.50 \text{ in.}^2$$

Thus

$$\dot{m} = \frac{3000 \times 83.50 \times 32.174}{7820} = 1031 \text{ lbm/s}$$

c) Mach number at exit M_e. Using Eq. (2.27) for the flow between the throat and exit of the nozzle, we have

$$\frac{A_e}{A_t} = \frac{1}{M_e}\left\{\frac{2}{\gamma+1}\left(1+\frac{\gamma-1}{2}M_e^2\right)\right\}^{\frac{\gamma+1}{2(\gamma-1)}} \tag{3.52}$$

This equation cannot be solved directly for the exit Mach number in terms of the area ratio A_e/A_t; however, it can be set into a form that permits fast iteration to the solution. Because there are two Mach numbers (a subsonic value and a supersonic value) that can give the same area ratio, we must be careful that we get the correct value. Solving Eq. (3.52) for the Mach number in the denominator gives an equation that will yield the subsonic Mach number corresponding to the area ratio A_e/A_t, or

Subsonic solution:

$$M_e = \frac{1}{A_e/A_t}\left\{\frac{2}{\gamma+1}\left(1+\frac{\gamma-1}{2}M_e^2\right)\right\}^{\frac{\gamma+1}{2(\gamma-1)}} \tag{3.53}$$

Equation (3.53) can be used to iterate on a solution for the subsonic exit Mach number by starting with a guess (say 0.5) and substituting it into the right-hand side of the equation and then solving for a new exit Mach number. The new value of the Mach number is substituted into the equation and another value of Mach number calculated. This iterative process is repeated until successive values do not change very much (say about 0.001).

The supersonic iteration equation for the exit Mach number is obtained from Eq. (3.52) by solving for the Mach number within the brace, or

Supersonic solution:

$$M_e = \sqrt{\frac{\gamma+1}{\gamma-1}\left\{M_e\frac{A_e}{A_t}\right\}^{\frac{2(\gamma-1)}{\gamma+1}} - \frac{2}{\gamma-1}} \tag{3.54}$$

The nozzle pressure ratio P_c/P_e is great enough to give supersonic flow at the exit, and iterative use of Eq. (3.54) gives the results tabulated in Table 3.11 starting with a guess of 4.0 for the exit Mach.

d) Nozzle design altitude. The nozzle design altitude corresponds to that altitude where $P_c = P_a$. With both the exit Mach number and the chamber pressure known, the nozzle exit pressure can be determined using Eq. (2.73) for P_t/P written as

$$P_e = P_c\left(1+\frac{\gamma-1}{2}M_e^2\right)^{-\gamma/\gamma-1} \tag{3.55}$$

Thus $P_e = 2.187$ psia.

Table 3.11 Solution to exit Mach

Guess M_e	Eq. (3.54)
4.0	4.9148
4.9148	5.0657
5.0657	5.0881
5.0881	5.0913
5.0913	5.0918
5.0918	5.0919
5.0919	5.0919

Thus $M_e = 5.0919$ (this answer can be found quickly using the GASTAB program).

This exit pressure corresponds to a value for the atmospheric pressure ratio δ of 0.1488 (=2.187/14.696). Using the Standard Atmospheric data of Appendix A, the nozzle design altitude is about 44,700 ft.

e) Nozzle separation altitude. The nozzle separation altitude corresponds to that altitude where $P_a = 3.5 \times P_{we} = 7.655$ psia. This pressure corresponds to a value for δ of 0.5209 (= 7.655/14.696). Using the Standard Atmospheric data of Appendix A, the nozzle separation altitude is about 17,000 ft.

f) Ideal thrust and thrust coefficient. The ideal thrust coefficient C_{Fi} is given by Eq. (3.44) in terms of γ, P_c/P_e, A_e/A_t, and P_a/P_c. Equation (3.41) gives the nozzle expansion ratio A_e/A_t in terms of the nozzle pressure ratio P_c/P_e. When the flow in the nozzle is not separated, both the nozzle expansion ratio A_e/A_t and the nozzle pressure ratio P_c/P_e will remain constant at their design values of 77 and 1372 (=3000/2.187), respectively. At altitudes below 17,000 ft, the flow in the nozzle will separate, and the effective nozzle expansion ratio A_e/A_t and nozzle pressure ratio P_c/P_e will be less than their design values.

The ideal thrust coefficient C_{Fi} and ideal thrust F_i will be obtained using Eqs. (3.44) and (3.43), respectively, and Eq. (3.41) will be used, when needed, to obtain the effective nozzle expansion ratio A_e/A_t. The required equations are Eq. (3.41):

$$\frac{A_e}{A_t} = \frac{\Gamma}{\sqrt{\dfrac{2\gamma}{\gamma - 1}\left[\left(\dfrac{P_e}{P_c}\right)^{\frac{2}{\gamma}} - \left(\dfrac{P_e}{P_c}\right)^{\frac{\gamma+1}{\gamma}}\right]}}$$

Eq. (3.44):

$$C_{Fi} = \Gamma\sqrt{\frac{2\gamma}{\gamma - 1}\left[1 - \left(\frac{P_e}{P_c}\right)^{\frac{\gamma-1}{\gamma}}\right]} + \left(\frac{P_e}{P_c} - \frac{P_a}{P_c}\right)\frac{A_e}{A_t}$$

Eq. (3.43):

$$F_i = C_{Fi} P_c A_t$$

The values of C_{Fi} vs altitude are plotted in Fig. 3.36, and values of thrust are plotted in Fig. 1.42b. Note the change in slope of the plots at the separation altitude. As expected, the actual thrust is increased by the flow separation at altitudes below 17,000 ft. This is one of the few times when nature is kind. Table 3.12 shows the ideal thrust coefficient and ideal thrust vs altitude of the SSME.

g) Calculate specific impulse in vacuum, $(I_{sp})_{vac}$. Using the definition of specific impulse given by Eq. (3.6), we write

$$(I_{sp})_{vac} = \frac{(F_i)_{vac} g_c}{\dot{m} g_o} = \frac{469{,}790 \times 32.174}{1030 \times 32.174} = 456.1 \text{ s}$$

h) Actual exhaust velocity V_e and effective exhaust velocity C at sea level. From Eq. (1.52), we can solve for the effective exhaust velocity C in terms of the thrust and mass flow rate to get

$$C = \frac{F_i g_c}{\dot{m}} = \frac{404{,}880 \times 32.174}{1030} = 12{,}647 \text{ ft/s}$$

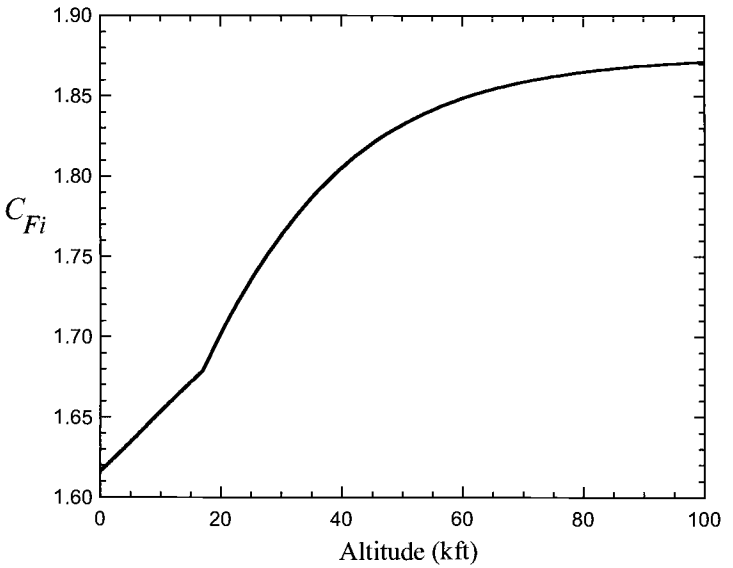

Fig. 3.36 Calculated ideal thrust coefficient of SSME.

Table 3.12 Ideal thrust coefficient and ideal thrust vs altitude of SSME

Altitude, ft	P_a, psia	P_e, psia	A_e/A_t	C_{Fi}	F_i, lbf
0	14.696	4.199	46.7	1.61627	404,880
5,000	12.228	3.494	53.8	1.63450	409,560
10,000	10.108	2.888	62.2	1.65345	414,190
15,000	8.297	2.371	72.4	1.67172	418,770
17,000	7.655	2.187	77.0	1.67892	420,570
20,000	6.759	2.187	77.0	1.70191	426,330
25,000	5.461	2.187	77.0	1.73523	434,670
30,000	4.373	2.187	77.0	1.76315	441,670
35,000	3.468	2.187	77.0	1.78638	447,490
40,000	2.730	2.187	77.0	1.80532	452,230
50,000	1.692	2.187	77.0	1.83197	458,910
60,000	1.049	2.187	77.0	1.84847	463,040
70,000	0.650	2.187	77.0	1.85871	465,610
80,000	0.404	2.187	77.0	1.86502	467,190
90,000	0.252	2.187	77.0	1.86893	468,170
100,000	0.160	2.187	77.0	1.87129	468,760
Vacuum	0	2.187	77.0	1.87540	469,790

Because we have determined the value of C_{Fi} at sea level and C^*, Eq. (3.51) can also be used to determine the effective exhaust velocity C at sea level. Substituting the values into Eq. (3.51) gives

$$C = C_{Fi}C^* = 1.61627 \times 7820 = 12{,}639 \text{ ft/s}$$

This value of C is about 0.06% lower than the value determined that can be attributed to roundoff.

The actual exhaust velocity V_e can be written in terms of the effective exhaust velocity using Eq. (1.51) as

$$V_e = C - (P_e - P_a)A_e g_c/\dot{m}$$

Using the value of C calculated and the values of P_e, P_a, and A_e/A_t determined in part f for sea level, the exhaust velocity can be calculated:

$$V_e = 12{,}647 - \frac{(4.199 - 14.696)(46.7 \times 83.50)32.174}{1030}$$

$$V_e = 12{,}647 + 1279 = 13{,}926 \text{ ft/s}$$

Example 3.8

Determine the C_{Fi} of the H-1 rocket engine at its design altitude of 80,000 ft using Fig. 3.31. The H-1 rocket engine has a chamber pressure P_c of 633 psia and a nozzle expansion ratio ε of 8. Assume $\gamma = 1.33$.

Solution: Using the standard atmosphere data in Appendix A at 80,000 ft, we get $P_a = 0.406$ psia and by calculation obtain $P_a/P_c = 0.00064$. Because the nozzle is at its design altitude, the flow is not separated in the nozzle. For $\varepsilon = 8$ and $\gamma = 1.33$, we have $(C_{Fi})_{\text{vac}} = 1.660$ from Fig. 3.31. For $\varepsilon = 8$ and $P_a/P_c = 0.00064$, we get $\Delta C_F = 0.005$. Thus,

$$C_{Fi} = (C_{Fi})_{\text{vac}} - \Delta C_F = 1.655$$

3.5.12 Liquid-Propellant Rockets

Liquid-propellant rockets can be classified into two general propellant categories: bipropellant (fuel and oxidizer) and monopropellant. Ordinarily, bipropellants are used for applications requiring high thrust, such as launch vehicles, and monopropellants are used for small control rockets. The focus in this section is on bipropellant rockets.

A typical liquid-propellant rocket consists of four main parts: rocket engine, propellants, propellant feed system, and propellant tanks. Figure 3.37 shows a schematic diagram of a bipropellant rocket with turbopump feed system. The turbopump feed system is usually used for high-thrust/long-duration rockets. In this system, fuel and oxidizer are burned in the gas generator. The resultant high temperature and pressure gas is expanded through the turbine before being exhausted. The turbine powers both the fuel and oxidizer pumps. This turbopump-fed rocket engine cycle is referred to as an *open cycle* because the working fluid exhausted from the turbine is discharged overboard. In *closed-cycle* turbopump feed systems, all of the working fluid exhausted from the turbine is injected into the combustion chamber of the rocket engine.

For a liquid-propellant rocket, the steady-state mass flow rate of propellant and combustion chamber pressure P_c are determined by a balance between mass flow rate entering the chamber from the fuel and oxidizer pumps and the mass flow rate leaving through the nozzle throat. The chamber pressure and mixture ratio of oxidizer to fuel directly affect the combustion process and its resultant products. For a given application, a high chamber pressure P_c is normally desirable because it permits higher nozzle thrust coefficient C_F and specific impulse I_{sp}. Most of the data presented in this section are for optimum expansion through a nozzle from a chamber pressure P_c of 1000 psia to an exhaust pressure P_e of 14.7 psia.

3.5.12.1 Propellants. Bipropellant liquid rockets use an oxidizer and a fuel. Typical oxidizers are liquid oxygen (O_2, also referred to as LOX), liquid fluorine (F), hydrogen peroxide (H_2O_2), chlorine trifluoride (ClF_3), nitric acid (HNO_3), and nitrogen tetroxide (N_2O_4). Common fuels include RP-1 (a hydrocarbon kerosene-like mixture), liquid hydrogen (H_2), hydrazine (N_2H_4), unsymmetrical dimethylhydrazine [$(CH_3)_2NNH_2$ also referred to as UDMH], monomethylhydrazine (CH_3NHNH_2), ethyl alcohol (C_2H_5OH), and liquid ammonia (NH_3). Table 3.13 shows some typical oxidizer/fuel combinations.

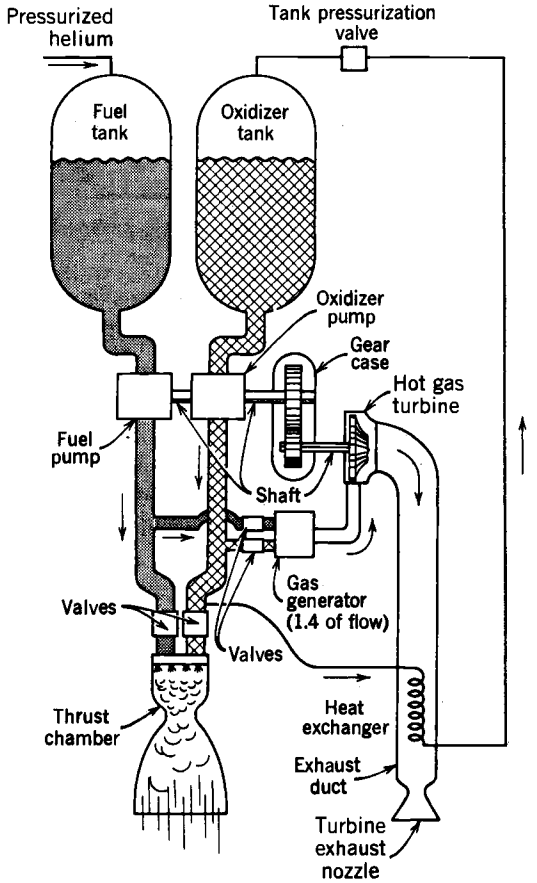

Fig. 3.37 Liquid-propellant rocket with turbopump feed system (from Ref. 19).

3.5.12.2 Performance calculations and results. It is beyond the scope of this chapter to cover the thermochemical theory and calculations required to determine the performance of a liquid-propellant rocket (see Chapter 2 for fundamentals). For the simple reaction between hydrogen (H_2) and oxygen (O_2), it is possible to form six products: water (H_2O), hydrogen (H_2), oxygen (H_2), hydroxyl (OH), atomic oxygen (O), and atomic hydrogen (H). The chemical equation for this reaction between a moles of hydrogen and b moles of oxygen can be written as

$$aH_2 + bO_2 \rightarrow n_{H_2O}H_2O + n_{H_2}H_2 + n_{O_2}O_2 + n_H H + n_O O + n_{OH}OH$$

Here n_{H_2O}, n_{H_2}, n_{O_2}, n_H, n_O, and n_{OH} are the molar quantities of the products.

Table 3.13 Theoretical performance[a] of liquid rocket propellant combinations[b] (from Ref. 19)

Oxidizer	Fuel	Mixture ratio		Chamber temperature, K	C^*, m/s	M, kg/mol	I_{sp}, s	γ
		By mass	By volume					
Oxygen:	75% Ethyl	1.30	0.98	3177	1641	23.4	267	1.22
	alcohol	1.43	1.08	3230	1670	24.1	279	
	Hydrazine	0.74	0.66	3285	1871	18.3	301	1.25
		0.90	0.80	3404	1892	19.3	313	
	Hydrogen	3.40	0.21	2959	2428	8.9	387	1.26
		4.02	0.25	2999	2432	10.0	390	
	RP-1	2.24	1.59	3571	1774	21.9	286	1.24
		2.56	1.82	3677	1800	23.3	300	
	UDMH	1.39	0.96	3542	1835	19.8	295	1.25
		1.65	1.14	3594	1864	21.3	310	
Fluorine:	Hydrazine	1.83	1.22	4553	2128	18.5	334	1.33
		2.30	1.54	4713	2208	19.4	363	
	Hydrogen	4.54	0.21	3080	2534	8.9	398	1.33
		7.60	0.35	3900	2549	11.8	410	
Nitrogen	Hydrazine	1.08	0.75	3258	1765	19.5	283	1.26
tetroxide:		1.34	0.93	3152	1782	20.9	292	
	50% UDMH	1.62	1.01	3242	1652	21.0	278	1.24
	50% hydrazine	2.00	1.24	3372	1711	22.6	288	
Red fuming	RP-1	4.10	2.12	3175	1594	24.6	258	1.22
nitric acid		4.80	2.48	3230	1609	25.8	268	
(15% NO_2):	50% UDMH-	1.73	1.00	2997	1682	20.6	272	1.22
	50% hydrazine	2.20	1.26	3172	1701	22.4	279	

[a]Conditions: $P_c = 1000$ psia, $P_e = 14.7$ psia, optimum nozzle expansion ratio, and frozen flow through nozzle.
[b]For every propellant combination, there are two sets of values listed: the upper line refers to frozen flow through the nozzle, the lower line to equilibrium flow through the nozzle.

An equilibrium solution of the preceding reaction in a combustion chamber can be obtained by use of the following principles:

1) Conservation of mass
2) Conservation of energy
3) Law of partial pressures

Figure 3.38 shows the results of these thermochemical calculations for liquid oxygen and the hydrocarbon fuel RP-1. Note that the concentration of carbon monoxide (CO) decreases and the oxidizer/fuel ratio is increased with a corresponding increase in carbon dioxide (CO_2). Also, note that the water (H_2O) reaches a maximum concentration for the given chamber pressure when the oxidizer/fuel ratio is about 2.7.

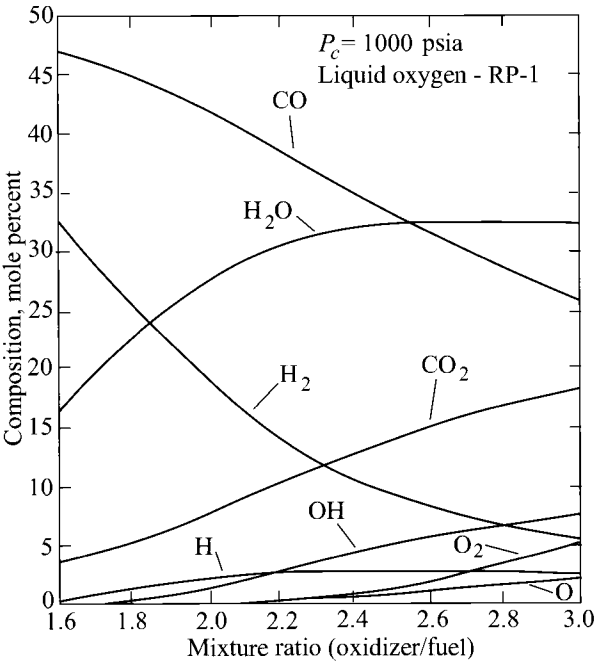

Fig. 3.38 Calculated chamber composition for liquid oxygen and RP-1 (from Ref. 19).

After reacting in the combustion chamber, the products then flow through the rocket nozzle. Two cases are considered for the flow of these products through the nozzle:

1) *Frozen flow*. The composition of the products do not change from those values determined for the combustion chamber. Here the mole fractions, molecular weight, etc., are the same at the nozzle exit as those at the exit of the combustion chamber.

2) *Equilibrium flow*. The composition of the products are maintained in chemical equilibrium as the pressure and temperature vary during the nozzle expansion process.

Figure 3.39 shows the equilibrium composition results leaving the nozzle for liquid oxygen and RP-1. Note that higher concentrations of carbon dioxide are shown in Fig. 3.39 leaving the nozzle than those shown leaving the combustion chamber in Fig. 3.38.

The actual flow through nozzles falls between these easily calculated cases. The products are able to stay in chemical equilibrium to some point downstream of the nozzle where their composition freezes. The equilibrium flow calculations give lower exhaust nozzle temperatures because of the recombination of dissociated species and thus give higher performance. Both frozen and equilibrium flow results are presented in Table 3.13.

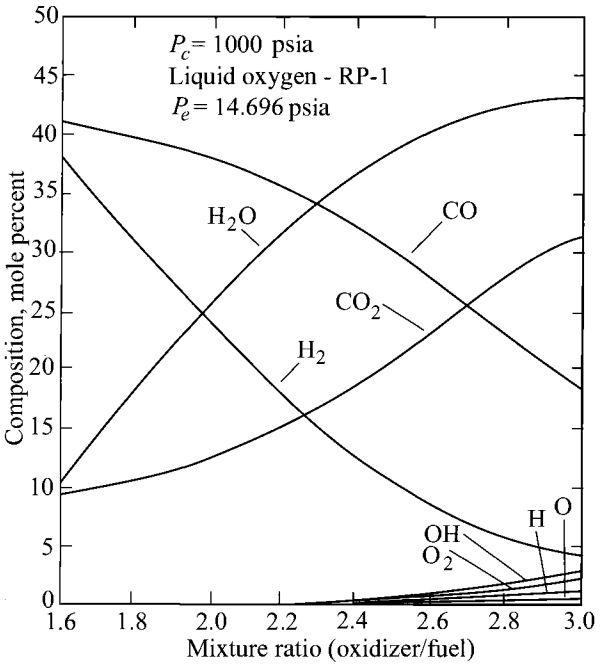

Fig. 3.39 Calculated nozzle exit equilibrium composition for liquid oxygen and RP-1 (from Ref. 19).

Example 3.9

Determine the I_{sp} of the oxygen-hydrogen rocket engine with a chamber temperature of 2960 K and an oxidizer-to-fuel mixture ratio by weight of 3.4:1 using the EQL software for both equilibrium and frozen flow through the nozzle. The rocket engine has a chamber pressure P_c of 1000 psia and an exit pressure P_e of 14.7 psia. Assume isentropic flow and perfect expansion.

Solution: The mixture ratio of 3.4:1 by weight equals a mole ratio of 0.214 (= 3.4 × 2.016/32). We use a pressure of 6893.2 kPa (= 1000 × 101.33/14.7) for the exit conditions from the combustion chamber. The nozzle inlet and exit states for both equilibrium and frozen flow are listed in Table 3.14. The exit velocity V_e follows from the definition of total enthalpy, Eq. (2.65).

3.5.13 Solid-Propellant Rockets

As shown in Fig. 3.40, solid-propellant rockets are relatively simple in construction. They contain the propellant to be burned within the combustion chamber or case. The propellant charge contains all of the chemical elements

Table 3.14 Oxygen–Hydrogen rocket engine results using EQL—Example 3.9

Property	Inlet	Exit, equilibrium flow	Exit, frozen flow
Pressure, kPa	6893.2	101.33	101.33
Temperature, K	2960.0	1308.3	1250.9
Molecular weight	8.80	8.87	8.80
Enthalpy, kJ/kg	371.3	−7835	−7651
V_e, m/s		4051	4006
I_{sp},		413	408

required for complete burning and is formed into a solid mass called the *grain.* Once the propellant is ignited, it burns on the surfaces of the propellant that are not inhibited by the case. The rate of burning is proportional to the exposed surface area.

3.5.13.1 Propellants. There are three general types of propellants for this type of rocket: double-base (homogeneous), composite (or heterogeneous), and composite modified double-base (CMDB). Table 3.15 gives representative formulations of these three types of propellants.

A homogeneous propellant has the fuel and oxidizer within the same molecule. The most common example of a homogeneous propellant is the double-base propellant of nitrocellulose and nitroglycerin with small amounts of additives. Figure 3.41 shows the variation in flame temperature and specific impulse with nitroglycerin (NG) concentration of the double-base propellant (JPN).

The composite propellant contains a heterogeneous mixture of oxidizer (as crystals) in a rubber-like binder. The binder is the fuel and must withstand a severe environment (high thermal and mechanical stresses). Hydroxyl terminated polybutaliene (HTPB) is a common binder. Common oxidizing crystals are ammonium perchlorate (AP), ammonium nitrate (AN), nitronium perchlorate (NP), potassium perchlorate (KP), potassium nitrate (KN), cyclotrimethylene trinitramine (RDX), and cyclotetramethylene tetranitramine (HMX).

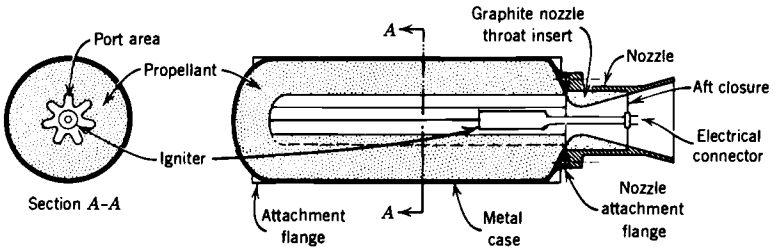

Fig. 3.40 Typical solid-propellant rocket motor (from Ref. 19).

Table 3.15 Representative propellant formulations in percent weight[a]

Propellant ingredient	Double-base (JPN)	Composite (PBAN)	Composite modified double-base (CMDB)
Nitrocellulose	51.5		21.9
Nitroglycerine	43.0		29.0
Ammonium perchlorate		70.0	20.4
Aluminum powder		16.0	21.1
Polybutadiene—acrylic acid—acrylonitrile		11.78	
Triacetin			5.1
Diethyl phthalate	3.2		
Epoxy curative		2.22	
Ethyl centralite	1.0		
Potassium sulfate	1.2		
Additives	0.1		
Stabilizers			

[a]Source: Air Force Wright Laboratory, Rocket Branch, Edwards, CA.

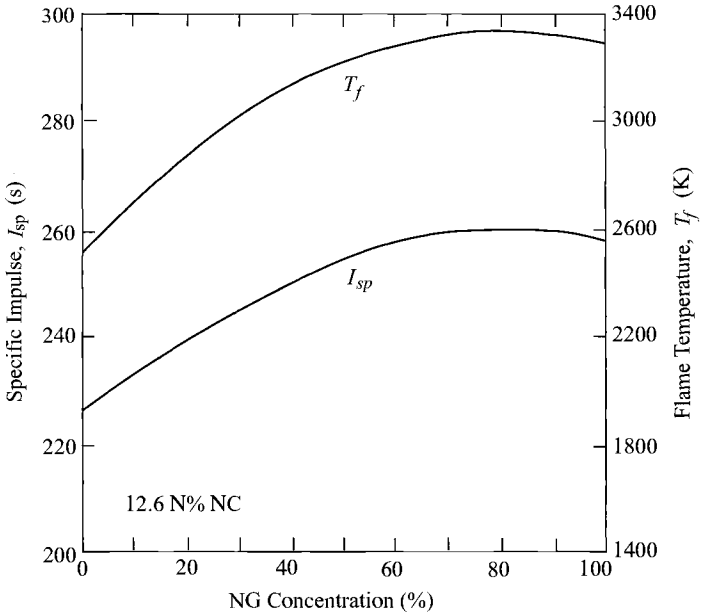

Fig. 3.41 Specific impulse and flame temperature vs nitroglycerin concentration of double-base propellants (from Ref. 21).

Figure 3.42 shows the variation in flame temperature, molecular weight, and specific impulse with oxidizer concentration for HTPB-based composite propellants. Maximum flame temperature for RDX and HMX are associated with 100% concentration, and these are commonly referred to as stoichiometrically balanced fuel-oxidizer combinations.

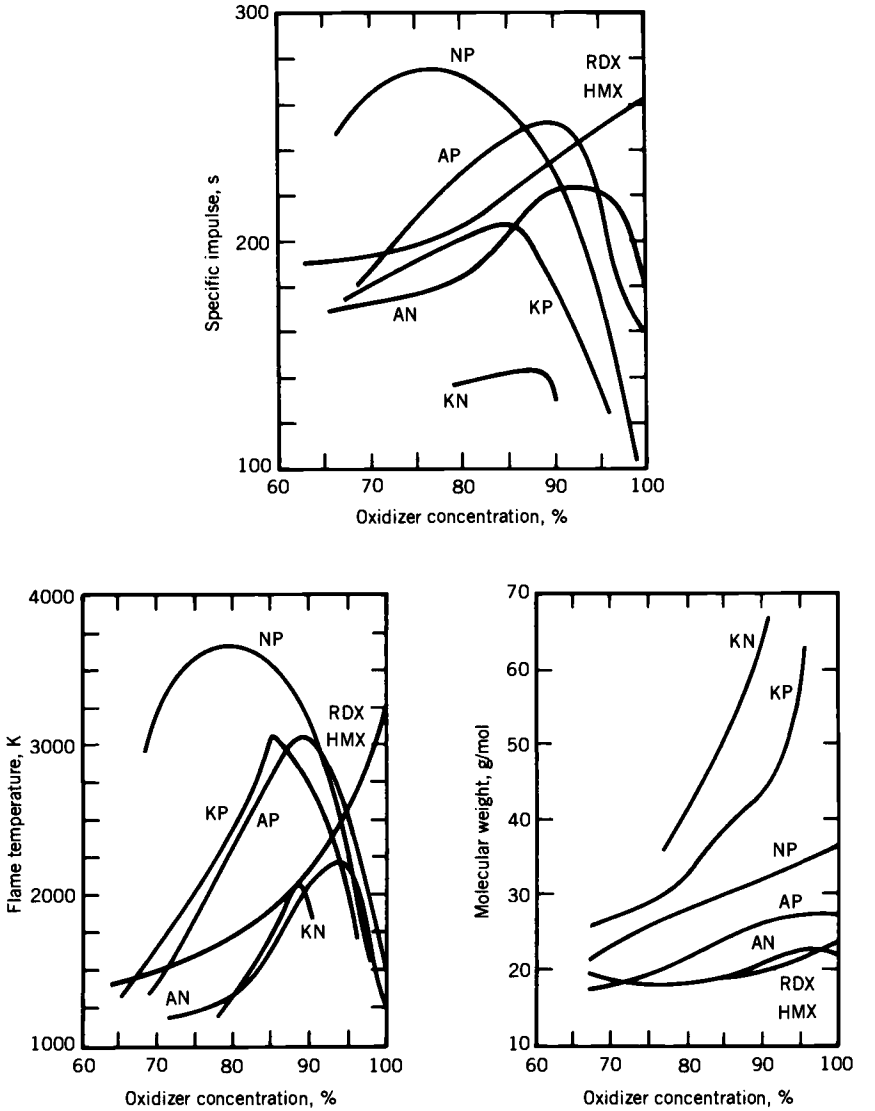

Fig. 3.42 HTPB-based composite propellants (from Ref. 21).

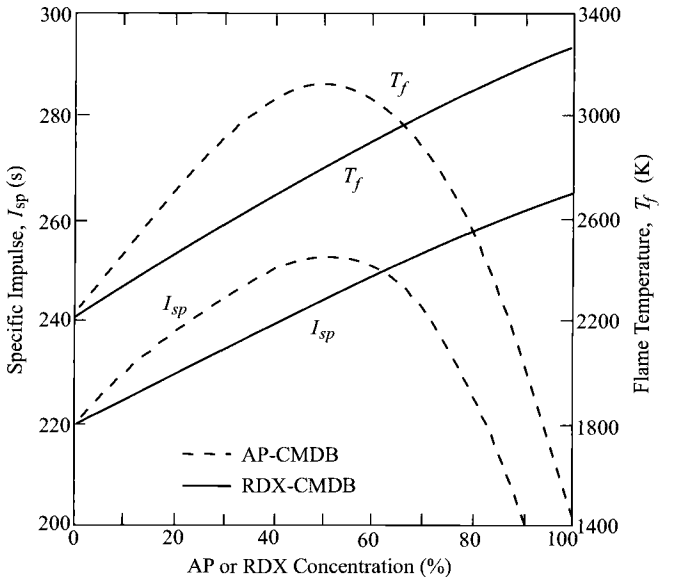

Fig. 3.43 Effects of percent concentration of AP or RDX on CMDB propellants (from Ref. 21).

The composite modified double-base (CMDB) propellant is a heterogeneous of the other two types of propellants. Figure 3.43 shows the variation in flame temperature and specific impulse vs the concentration of AP and RDX in AP-CMDB and RDX-CMDB propellants.

Metal powders are commonly added to solid propellants to increase specific impulse and fuel density. Aluminum powders that constitute 12–20% of the propellant mass have given the most successful experience.

The theoretical performances of three solid propellants are presented in Table 3.16. The results for specific impulse I_{sp} and effective exhaust velocity C are based on frozen flow through an optimum nozzle expansion ratio from a chamber pressure of 1000 psia to an exhaust pressure of 14.7 psia.

3.5.13.2 Burning rate. The burning rate r for a solid propellant is defined as the recession of the propellant surface per unit time (see Fig. 3.44). The burning rates of typical solid propellants are given in Fig. 3.45. For a given solid propellant, this rate is mainly a function of the chamber pressure P_c and is commonly written as

$$r = aP_c^n \tag{3.56}$$

where a is an empirical constant influenced by the ambient temperature of the propellant prior to ignition, and n is known as the *burning rate pressure exponent.*

Table 3.16 Theoretical performance of typical solid-rocket propellant combinations[a] (from Ref. 19)

Oxidizer	Fuel	Chamber temperature, K	C^*, m/s	$\mathcal{M}$, kg/mol	I_{sp}, s	γ
Ammonium nitrate	11% binder and 7% additives	1282	1209	20.1	192	1.26
Ammonium perchlorate 78–66%	18% organic polymer binder and 4–20% aluminum	2816	1590	25.0	262	1.21
Ammonium perchlorate 84–68%	12% polymer binder and 4–20% aluminum	3371	1577	29.3	266	1.17

[a]Conditions for I_{sp} and C: $P_c = 1000$ psia, $P_e = 14.7$ psia, optimum nozzle expansion ratio, and frozen flow through nozzle.

When a single value of the burning rate is given, this value corresponds to a propellant ambient temperature of 70°F and a combustion pressure of 1000 psia unless otherwise stated. For the composite ammonium nitrate propellant curve in Fig. 3.45, corresponding to an ambient temperature of −40°F, the empirical constants a and n are 0.0034 in./s and 0.445, respectively, for the chamber pressure P_c expressed in units of psia.

Accounting for both the density of the solid propellant and that of the propellant gas, the net mass flow rate of propellant gas being generated can be expressed as

$$\dot{m} = (\rho_s - \rho_g) r A_b \tag{3.57}$$

where A_b is the burning area of the propellant, r the burning rate, ρ_s the solid propellant density at ambient temperature, and ρ_g the propellant gas density. Since A_b and r vary with time and chamber pressure P_c, the thrust of a solid-propellant rocket changes with time. The variation in burning area of the propellant A_b designed into the grain determines the variation in thrust over time. Figure 3.46 shows six grain designs, their variations in thrust with time, and the corresponding general category of thrust variation.

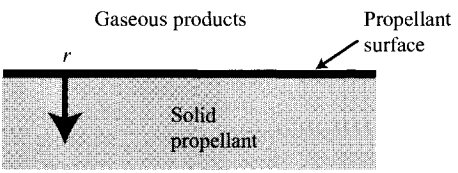

Fig. 3.44 Burning of a solid propellant.

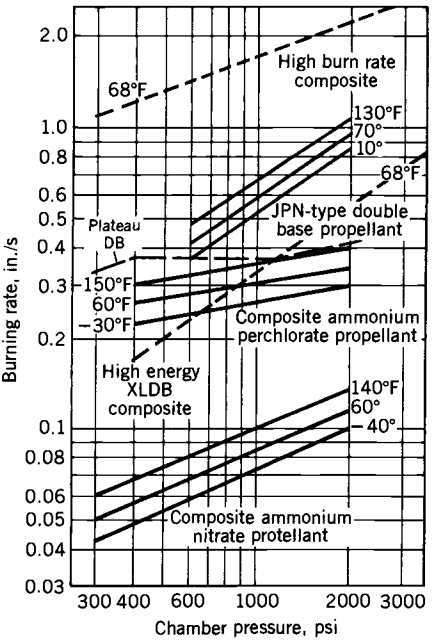

Fig. 3.45 Burning rates of typical solid propellants (from Ref. 19).

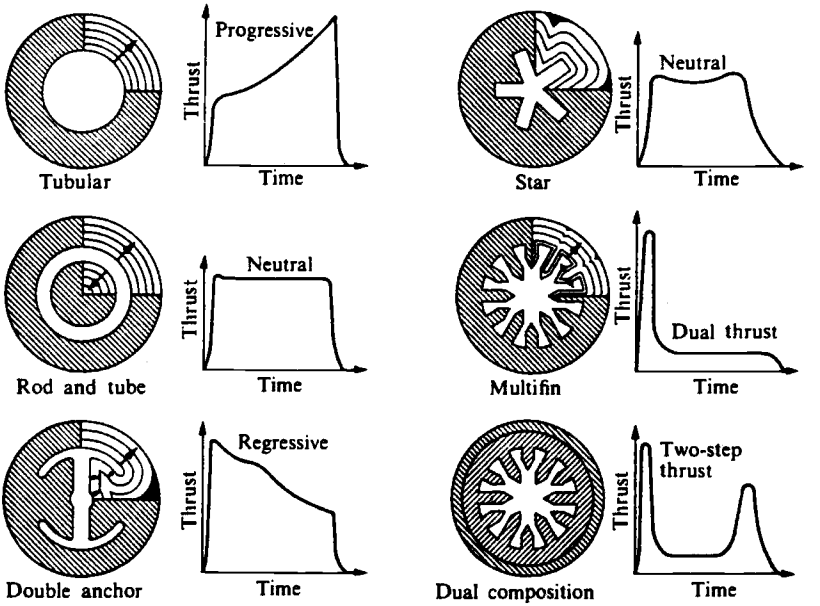

Fig. 3.46 Grain design and thrust vs time (from Ref. 22).

3.5.13.3 Chamber pressure and stability. A steady-state chamber pressure P_c is reached when the net mass flow of propellant gas being generated equals the mass flow rate of propellant gas leaving the nozzle. Using Eqs. (3.36), (3.38), and (3.57), we write

$$\dot{m} = \frac{P_c A_t g_c}{C^*} = (\rho_s - \rho_g) r A_b$$

where A_t is the nozzle throat area and C^* is the characteristic velocity given by Eq. (3.38). For solid-propellant rockets, the characteristic velocity C^* depends mainly on the propellant. Substituting the empirical relationship of Eq. (3.56) for the burning rate r into the preceding equation gives

$$\dot{m} = \frac{P_c A_t g_c}{C^*} = (\rho_s - \rho_g) a P_c^n A_b \tag{i}$$

Plotting the nozzle mass flow rate and propellant gas generation rate vs the chamber pressure gives the general curves shown in Fig. 3.47. Two curves are drawn for the propellant gas generation rate (mass burn rate): one for $n < 1$ and another for $n > 1$. *Stability requires that burning rate pressure exponent n be less than unity.* If n is greater than unity, increases in chamber pressure above operating point will cause the propellant gas generation to increase faster than the nozzle flow rate. The result would lead to a rapid rise in chamber pressure with an accompanying explosion.

From Eq. (i), the chamber pressure P_c can be expressed as

$$P_c = \left\{ \frac{a(\rho_s - \rho_g) C^*}{g_c} \frac{A_b}{A_t} \right\}^{\frac{1}{1-n}} \tag{3.58}$$

This equation can be used to determine the chamber pressure when data are available for the terms on the right-hand side of the equation. Because the density

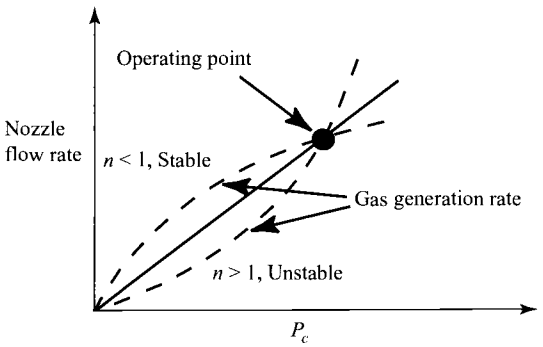

Fig. 3.47 Mass flow rate vs chamber pressure.

of the propellant gas is much smaller than that of the solid propellant, it is often neglected and Eq. (3.58), written as

$$P_c = \left\{ \frac{a\rho_s C^* A_b}{g_c A_t} \right\}^{\frac{1}{1-n}} \tag{3.59}$$

The sensitivity of the chamber pressure P_c to changes in the burn-to-throat area ratio A_b/A_t can be investigated with this equation. As an example, for a burning rate pressure exponent n of 0.75, the change in chamber pressure is proportional to A_b/A_t raised to the fourth power, which can lead to large variations in P_c over the burn. It is for this reason that most propellants have burning rate pressure exponent n in the range of 0.2 to 0.3.

As an example of the use of Eq. (3.59) to determine chamber pressure P_c, we consider a solid-propellant rocket with $A_b/A_t = 600$. The properties for the propellant are $\rho_s = 0.06$ lbm/in.^{3}, $n = 0.2$, $a = 0.05$ in./s, and $C^* = 5000$ ft/s. Using Eq. (3.59) gives

$$P_c = \left\{ \frac{0.05 \times 0.06 \times 5000}{32.174} 600 \right\}^{1.25} = 1144 \text{ psia}$$

Equation (3.59) can be used to determine the burn-to-throat area ratio A_b/A_t of a solid-propellant rocket when the other data are known. Solving Eq. (3.59) for this area ratio gives

$$\frac{A_b}{A_t} = \frac{g_c}{a\rho_s C^*} P_c^{1-n} \tag{3.60}$$

Consider that a chamber pressure 2000 psia is desired for the same propellant as used in the preceding. The required burn-to-throat area ratio is

$$\frac{A_b}{A_t} = \frac{32.174}{0.05 \times 0.06 \times 5000} 2000^{0.8} = 938$$

3.5.13.4 Total impulse and times. The total impulse I_t of a rocket is the integral of the thrust over the burning time t_b, or

$$I_t = \int_0^{t_b} F \, dt = \overline{F} t_b \tag{3.61}$$

where $\overline{F}$ is the average thrust over the burning time t_b, which is defined in Fig. 3.48, along with the action time t_a. Figure 3.48 shows representative plots of experimentally measured chamber pressure P_c vs time.

The specific impulse, effective exhaust velocity, and propellant mass flow rate cannot be measured directly in an experiment. The normal procedure is to determine the average specific impulse by finding the total impulse I_t and

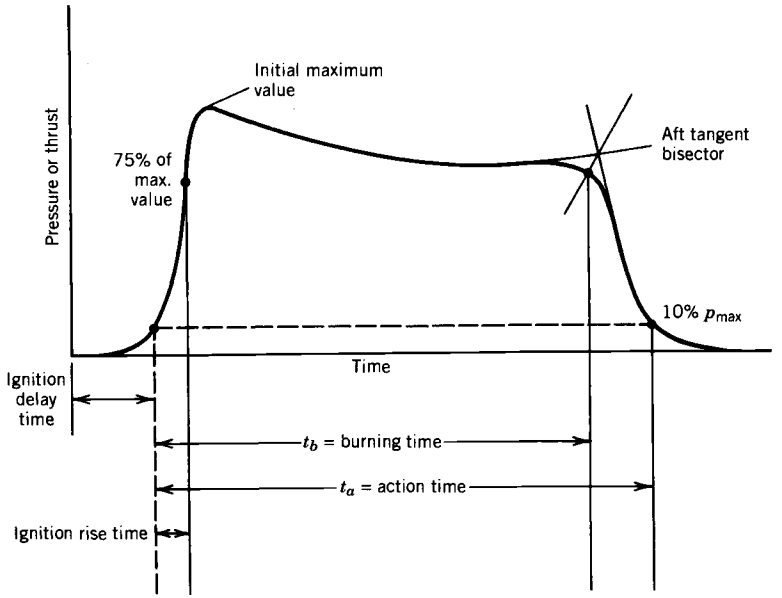

Fig. 3.48 Definition of burning time t_b and action time t_a (from Ref. 19).

weight of propellant w used for a rocket test. The average specific impulse ($\overline{I_{sp}}$) is then given by

$$\overline{I_{sp}} = \frac{I_t}{w} \tag{3.62}$$

The average effective exhaust velocity $\overline{C}$ and mass flow rate $\overline{\dot{m}}$ then follow from Eq. (3.6) and the values for the weight of propellant w used and burning time t_b. Thus we have

$$\overline{C} = \overline{I_{sp}} g_o \tag{3.63}$$

$$\overline{\dot{m}} = \frac{w}{t_b} \frac{g_c}{g_o} \tag{3.64}$$

Example 3.10

Two tests of a 5-in. diam, center-perforated, solid-propellant rocket was performed at the United States Air Force Academy. The first test used a convergent-only nozzle, and the second test used a convergent-divergent nozzle. Figure 3.49 shows a sketch of the test rocket motors. The rocket propellant grain burns on both ends and in the center. The following data were provided by the manufacturer:

1) Ammonium perchlorate composite propellant with aluminum (70% NH_4ClO_4, 15% Al, 15% binder),

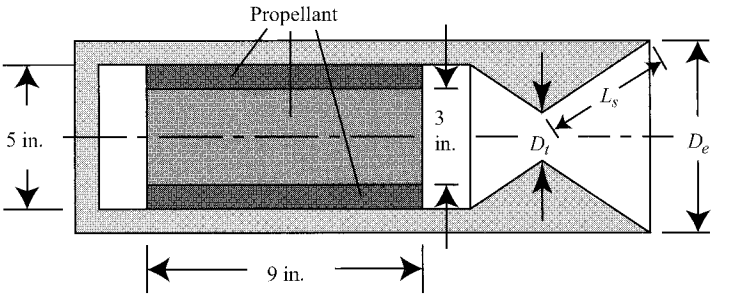

Fig. 3.49 Sketch of test rocket motor with convergent-divergent nozzle.

2) $C^* = 5118$ ft/s, $\mathcal{M} = 25.55$, $\gamma = 1.2$, $\rho_s = 0.064$ lbm/in.^{3},
3) Burning rate coefficients: $a = 0.0773$ in./s, $n = 0.21$, P_c in psia.

The test data for the two tests are presented in Table 3.17. The results for Case I are calculated and discussed in the following. The calculations for Case II are left as a homework problem.

Case I results:

$$\text{Average thrust} = \overline{F} = \frac{I_t}{t_b} = \frac{1257.6}{4.113} = 305.8 \text{ lbf}$$

$$\text{Average } P_c = \overline{P}_c = \int_0^{t_b} (P_c - P_a)\, dt/t_b + P_a$$

$$= 1161.6/4.113 + 23.16 \times 0.491 = 293.8 \text{ psia}$$

$$\text{Average } A_t = \overline{A_t} = \pi(1.1075)^2/4 = 0.963 \text{ in.}^2$$

$$\text{Burning rate} = r = a(\overline{P}_c)^n = 0.0773(293.8)^{0.21} = 0.255 \text{ in./s}$$

Table 3.17 Test data of two small solid-propellant rockets

Item	Case I	Case II
Barometric pressure P_a, in Hg	23.16	23.33
Initial rocket case weight, lbf	17.42	17.35
Final rocket case weight, lbf	10.10	10.10
Nozzle type	Convergent	Convergent-divergent
Initial throat diameter d_t, in.	1.107	0.852
Final throat diameter d_t, in.	1.108	0.866
Exit diameter d_e, in.	N/A	2.225
Nozzle slant length L_s, in.	N/A	3.0
Burning time t_b, s	4.113	3.64
$\int_0^{t_b} (P_c - P_a)\ dt$, psig-s	1161.6	1921.6
$I_t = \int_0^{t_b} F\ dt$, lbf-s	1257.6	1570.8

$$\text{Average burning rate} = \bar{r} = \frac{\text{Web thickness}}{t_b} = \frac{1.00}{4.113} = 0.243 \text{ in./s}$$

$$\text{Initial burning surface} = A_b = 2\pi(r_i L + r_o^2 - r_i^2)$$
$$= 2\pi(1.5 \times 9 + 2.5^2 - 1.5^2) = 110 \text{ in.}^2$$

$$\text{Initial propellant flow rate} = \dot{m} = r\rho_s A_b$$
$$= 0.255 \times 0.064 \times 110 = 1.795 \text{ lbm/s}$$

$$\text{Average propellant flow rate} = \bar{\dot{m}} = \frac{wg_c}{t_b g_o} = \frac{7.32}{4.113}\frac{32.174}{32.174} = 1.780 \text{ lbm/s}$$

$$\text{Experimental } C^* = \frac{\overline{P_c}\,\overline{A_t} g_c}{\bar{\dot{m}}} = \frac{293.8 \times 0.963 \times 32.174}{1.780} = 5114 \text{ ft/s}$$

$$\text{Experimental } C_F = \frac{\bar{F}}{\overline{P_c}\,\overline{A_t}} = \frac{305.8}{293.8 \times 0.963} = 1.081$$

$$\text{Experimental } I_{sp} = \frac{I_t}{w} = \frac{1257.6}{7.32} = 171.8 \text{ s}$$

$$\text{Experimental } C = I_{sp} g_o = 171.8 \times 32.174 = 5527 \text{ ft/s}$$

Theoretical thrust coefficient: $\gamma = 1.2$, $\varepsilon = 1$

$$\frac{P_c}{P_a} = \frac{293.8}{23.16 \times 0.491} = 25.84, \quad \frac{P_c}{P_e} = \left(\frac{\gamma+1}{2}\right)^{\gamma/(\gamma-1)} = \left(\frac{2.2}{2}\right)^6 = 1.772$$

Using these data with Eq. (3.44) gives $C_F = 1.185$, and

$$\text{Ideal } C = C_F C^* = 1.185 \times 5118 = 6065 \text{ ft/s}$$

$$\text{Ideal } I_{sp} = \frac{C}{g_o} = \frac{6065}{32.174} = 188.5 \text{ s}$$

The experimental and manufacturer's values of C^* are the same. The average and initial burning rates are within 5% of each other. The average and initial mass flow rates are within 1% of each other. Closer agreement between experimental and ideal results could be obtained with a higher γ.

Problems

3.1 For propellants having a specific impulse of 360 s, determine the mass flow rate through a rocket nozzle to obtain a thrust of 10,000 N.

3.2 For propellants having a specific impulse of 265 s, determine the mass flow rate through a rocket nozzle to obtain a thrust of 1,500,000 lbf.

3.3 Exhaust gas with $R = 0.375$ kJ/kg-K and $\gamma = 1.26$ flows through an isentropic nozzle. If the gas enters the nozzle at 100 atm and 4000 K and exits to a pressure of 1 atm, determine the following for a choked nozzle throat:
(a) the exhaust velocity V_e

(b) the specific impulse I_{sp}
(c) mass flow rate and ideal thrust for a throat area A_t of 0.1 m^2

3.4 Determine the area ratio of the nozzle in Problem 3.3.

3.5 Determine the gross weight at liftoff for a single-stage rocket with a 2000-kg payload placed in a low Earth orbit using a liquid O_2-H_2 propulsion system. Assume a burn time of 100 s and an average specific impulse of 400 s.

3.6 Determine the gross weight at liftoff for a single-stage rocket with a 1000-kg payload placed in a low Earth orbit using a liquid O_2-kerosene propulsion system. Assume a burn time of 120 s and an average specific impulse of 310 s.

3.7 Rework Example 3.3 with a liquid O_2-kerosene propulsion system having an average specific impulse of 310 s.

3.8 A calorically perfect gas with a molecular weight of 18 and $\gamma = 1.25$ has a combustion temperature T_c of 6000°R. Determine the characteristic velocity C^*.

3.9 Determine the characteristic velocity C^* for the data of Example 3.5.

3.10 Determine the area ratio (A_e/A_t) for a rocket nozzle operating at a pressure ratio (P_c/P_e) of 1000 with a calorically perfect gas where $\gamma = 1.2$.

3.11 A rocket nozzle has an ideal thrust coefficient C_{Fi} of 1.5, a chamber pressure P_c of 100 atm, and a throat area A_t of 0.15 m^2. Determine the ideal thrust F_i.

3.12 A rocket nozzle has an area ratio (A_e/A_t) of 25. If a calorically perfect gas with $\gamma = 1.25$ flows through the nozzle, determine its pressure ratio (P_c/P_e) and ideal thrust coefficient in a vacuum $(C_{Fi})_{vac}$.

3.13 Find the ideal thrust coefficient C_{Fi} for a rocket at 50-km altitude with an area ratio of 50, $\gamma = 1.28$, and a chamber pressure $P_c = 40$ atm.

3.14 Calculate the ideal thrust coefficient C_{Fi} and ideal thrust F_i for the space shuttle main engine (SSME) data of Example 3.7 at an altitude of 45,000 ft.

3.15 A chemical rocket motor has the following data during static testing at sea level:

$P_c = 225$ atm, $T_c = 2800$ K, $M_e = 5.3$
$\varepsilon = 62$, exit diameter = 2.15 m

Assume a calorically perfect gas with $\gamma = 1.3$ and $R = 0.317$ kJ/kg-K. Determine the throat area A_t, exit pressure P_e, exit temperature T_e, exit velocity V_e, mass flow rate $\dot{m}$, and thrust at both sea-level and design altitude.

3.16 A rocket booster using H_2-O_2 requires an ideal thrust of 100,000 lbf at a design altitude of 80 kft. The booster will have a chamber temperature of 4840°R and a throat area of 0.5 ft^2. Assuming a specific impulse of 400 s and a calorically perfect gas with $\gamma = 1.26$ and $R = 173.6$ ft-lbf/lbm-°R, determine the following:

(a) Mass flow rate
(b) Characteristic velocity C^*
(c) Chamber pressure P_c
(d) Effective exhaust velocity C at 80-kft altitude
(e) Ideal thrust coefficient C_{Fi} at 80-kft altitude
(f) Nozzle expansion ratio ε and exit diameter
(g) Altitude that flow in the nozzle is just separated (assume separation when $P_a > 3.5\ P_{we}$)
(h) Ideal thrust at sea level

3.17 Determine the I_{sp} of the oxygen-hydrogen rocket engine with a chamber temperature of 3200 K and an oxidizer-to-fuel mixture ratio by weight of 3.0:1 using the EQL software for both equilibrium and frozen flow through the nozzle. The rocket engine has a chamber pressure (P_c) of 100 atm and an exit pressure P_e of 1 atm. Assume isentropic flow and perfect expansion.

3.18 A solid-propellant rocket has $\rho_s = 0.06$ lbm/in.^{3}, $n = 0.2$, $a = 0.05$ in./s, and $C^* = 5000$ ft/s. Determine the burn-to-throat area ratio (A_b/A_t) for a chamber pressure of 1500 psia.

3.19 Determine the performance of Case II in Table 3.17. Compare your results to Case I (Example 3.10).

3.20 From a search of the Internet, find a thrust vs time plot for a solid-propellant motor (e.g., Estes Rocket Motors) and determine the burning time, action time, impulse, average mass flow rate, and average thrust.

3.21 Test firing of a 2.75-in. solid rocket at the U.S. Air Force Academy on May 8, 1992, gave the data plotted in Fig. P3.1.[23] The rocket motor used was the "Mighty Mouse" solid-propellant system used for the air-to-ground 2.75-in. folding fin aerial rocket. The motor uses a Class B propellant (MK43 MOD 1 propellant grain) with an internal burning eight-point star grain configuration. The motor has four straight, fixed, conical nozzles. The physical characteristics and published performance of the Mighty Mouse rocket motor based on 70°F sea-level operation are as follows:

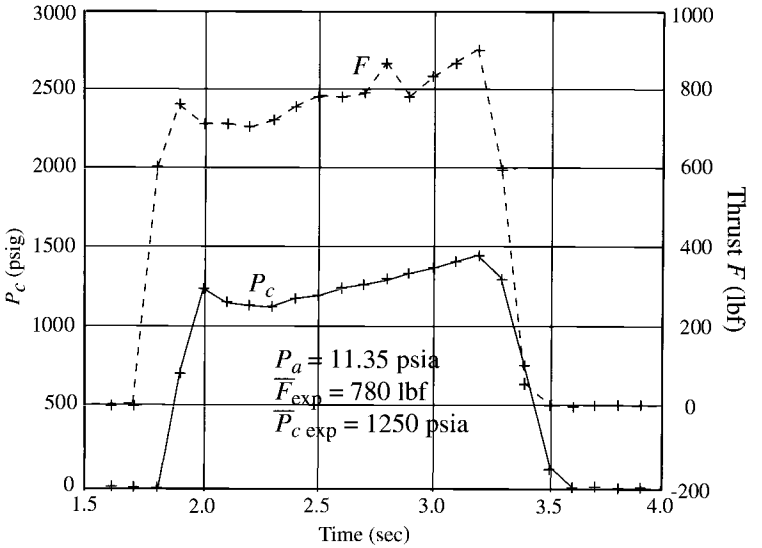

Fig. P3.1 Test firing of a 2.75-in. solid rocket at the U.S. Air Force Academy on May 8, 1992 (Ref. 23).

Size and mass:
Overall length = 39.4 in., nominal diameter = 2.75 in., loaded mass = 11.37 lbm, expended mass = 5.9 lbm, propellant mass = 6.40 lbm, and initial area of propellant burning surface = 160.83 in.^{2}

Manufacturer's performance characteristics (70°F sea-level operation):

Average chamber pressure P_c	1210 psia
Motor specific impulse	103 lbf-s/lbm
Action time impulse	1140 lbf-s
Total impulse	1170 lbf-s
Propellant	NC/NG/DEP/other (50/36/11/4%)
Propellant specific impulse I_{sp}	183 s
Propellant density ρ_p	0.056 lbm/in.^{3}
Propellant burn rate (1000 psia), r	0.48 in./s
Ratio of specific heat for gas, γ	1.17
Propellant mass fraction	0.563
Total nozzle throat area, A^*	0.444 in.^{2}
Expansion cone half angle	10°15′
Nozzle expansion ratio ε	3.75
Characteristic exhaust velocity C^*_{manuf}	4159 ft/s
Thrust coefficient, C_F	1.415

(a) Calculate the exit Mach number M_e.
(b) Using the experimental chamber pressure $P_{c\ exp}$ and calculated exit Mach number, calculate the exit pressure P_e.
(c) Describe the exit flow as underexpanded or overexpanded (see Figs. 2.37 and 2.38).
(d) Calculate the mass flow rate of the combustion products based on the initial area of propellant burning surface.
(e) Calculate the characteristic exhaust velocity C^*_{exp} based on the mass flow rate of item c and the experimental chamber pressure $P_{c\,exp}$.
(f) Calculate the thrust coefficient $C_{F\text{calc}}$ using the measured thrust and chamber pressure $P_{c\,exp}$.
(g) Calculate the thrust produced by the rocket using the calculated thrust coefficient, measured chamber pressure, and nozzle throat area.
(h) Calculate the experimental specific impulse $I_{sp\,exp}$.
(i) Compare calculated results to manufacturer's performance characteristics.